

1 **Investigation of the summer 2018 European ozone air pollution episodes using**
2 **novel satellite data and modelling**

3 Richard J. Pope^{1,2}, Brian J. Kerridge^{3,4}, Martyn P. Chipperfield^{1,2}, Richard Siddans^{3,4}, Barry G. Latter^{3,4},
4 Lucy J. Ventress^{3,4}, Matilda A. Pimlott¹, Wuhu Feng^{1,5}, Edward Comyn-Platt⁶, Garry D. Hayman⁷,
5 Stephen R. Arnold¹ and Ailish M. Graham¹

6
7 *1: School of Earth and Environment, University of Leeds, Leeds, United Kingdom*

8
9 *2: National Centre for Earth Observation, University of Leeds, Leeds, United Kingdom*

10
11 *3: Remote Sensing Group, STFC Rutherford Appleton Laboratory, Chilton, United Kingdom*

12
13 *4: National Centre for Earth Observation, STFC Rutherford Appleton Laboratory, Chilton, United*
14 *Kingdom*

15
16 *5: National Centre for Atmospheric Science, University of Leeds, Leeds, United Kingdom*

17
18 *6: European Centre for Medium-Range Weather Forecasts, Reading, UK*

19
20 *7: Centre for Ecology and Hydrology, Wallingford, United Kingdom*
21

22 Submitted to *Atmospheric Chemistry and Physics*

23 Correspondence to: Richard J. Pope (r.j.pope@leeds.ac.uk)

24 **Abstract:**

25 In the summer of 2018, Europe experienced an intense heat wave which coincided with several
26 persistent large-scale ozone (O₃) pollution episodes. Novel satellite data of lower tropospheric
27 column O₃ from the Global Ozone Monitoring Experiment-2 (GOME-2) and Infrared Atmospheric
28 Sounding Interferometer (IASI) on the MetOp satellite showed substantial enhancements in 2018
29 relative to other years since 2012. Surface observations also showed ozone enhancements across
30 large regions of continental Europe in summer 2018 compared to 2017. Enhancements to surface
31 temperature and the O₃ precursor gases carbon monoxide and methanol in 2018 were co-retrieved
32 from MetOp observations by the same scheme. This analysis was supported by the TOMCAT
33 chemistry transport model (CTM) to investigate processes driving the observed O₃ enhancements.
34 Through several targeted sensitivity experiments we show that meteorological processes, and
35 emissions to a secondary order, were important for controlling the elevated O₃ concentrations at the
36 surface. However, mid-tropospheric (~500 hPa) O₃ enhancements were dominated by
37 meteorological processes. We find that contributions from stratospheric O₃ intrusions ranged
38 between 15 - 40%. Analysis of back trajectories indicates that the import of O₃-enriched air masses
39 into Europe originated over the North Atlantic substantially increasing O₃ in the 500 hPa layer during
40 summer 2018.

43 **1. Introduction**

44 Over the past two decades there have been several intense summer-time heatwaves over Europe
45 (e.g. 2003 over continental Europe (Scott et al., 2004), 2006 over north-western Europe (Rebetez et
46 al., 2008) and 2010 across eastern Europe and Russia (Matsueda et al., 2011)). With current and
47 future climate change, increasing average global surface temperature is expected to trigger more
48 frequent and intense heatwaves (Lhotka et al., 2017; Guerreiro et al., 2018). The summer-time 2018
49 heatwave across predominantly north-western and central Europe and Scandinavia generated
50 temperature anomalies of approximately 2.0-4.0 K (Li et al., 2020; Drouard et al., 2020). Dynamically,
51 it was caused by a combination of intense anticyclonic blocking systems, Rossby wave dynamics and
52 the positive phase of the summer-time North Atlantic Oscillation (NAO+) (Li et al., 2020; Liu et al.,
53 2020; Drouard et al., 2020). Environmentally, the summer 2018 heatwave caused severe drought
54 conditions with decreased precipitation and soil moisture content (Bastos et al., 2020; Dirmeyer et
55 al., 2020), while negatively impacting natural vegetation (e.g. decreased gross primary productivity
56 (Smith et al., 2020; Bastos et al., 2020)). From a human health perspective, the 2018 heatwave
57 caused 863 temperature related excess deaths in the UK (PHE, 2019).

58 As well as meteorological and vegetation responses, enhancements in atmospheric pollutants from
59 heatwaves can lead to a degradation in air quality (AQ) across Europe. Blocking systems (anticyclonic
60 conditions) have been shown to increase the level of air pollutions such as carbon monoxide (CO;
61 Thomas and Devasthale, 2014), nitrogen dioxide (NO₂; Pope et al., 2014) and particulate matter (i.e.
62 PM_{2.5}; Graham et al., 2020) to hazardous levels. Pope et al., (2016) focused on the 2006 UK
63 heatwave and detected enhancements in surface O₃ through the accumulation of pollutants (i.e.
64 atmospheric blocking) but also the higher temperatures yielding more active atmospheric chemistry
65 (i.e. ozone formation). Papanastasiou et al., (2015) found that Greek heatwave conditions (2001-
66 2010) typically yielded an increase in NO₂, PM_{2.5} and O₃ by 14-29%, 25-38% and 12%, respectively.
67 Rasilla et al., (2019) found that heatwaves in Madrid only moderately increased NO₂ and O₃ but
68 significantly increased PM₁₀ concentrations. However, they associated this with enhanced long-
69 range transport of African dust and then accumulation under heatwave conditions. García-Herrera et
70 al., (2010) provided a review of the 2003 European heatwave finding that the Alpine region had
71 substantially elevated surface ozone levels (peaking at 417 µg/m³ with 68% of sites from 23
72 countries reaching concentrations above 180 µg/m³) when compared with the previous 12 summers.
73 Biogenic volatile organic compound (BVOC) emissions from vegetation are known to increase under
74 drought conditions from temperature stress (e.g. in the 2003 European heatwave; Rennenberg et
75 al., 2006). Churkina et al., (2017) found that heatwave conditions (2006) in Berlin yielded an increase
76 in BVOC emissions which contributed up to 12% of the surface ozone formation. Heatwaves can also
77 trigger wildfires, which emit primary air pollutions and can form secondary gases such as surface
78 ozone on a regional and hemispheric scale (Honrath et al., 2004). Overall, elevated surface O₃ is
79 associated with adverse health impacts (Doherty et al., 2017; Heal et al., 2013; Jerrett et al., 2009)
80 with ailments such as asthma, reduced lung function and disease (WHO, 2021). It also has adverse
81 impacts on the natural biosphere (Sitch et al., 2007) and agriculture (Hollaway et al., 2012; van
82 Dingenen et al., 2009), in turn reducing deposition of surface ozone on vegetation. As well as
83 dynamical and vegetation responses, enhancements in atmospheric pollutants from heatwaves can
84 lead to a degradation in air quality (AQ). Firstly, anticyclonic conditions (i.e. atmospheric blocking)
85 have been shown to cause the accumulation of primary air pollutants such as carbon monoxide (CO;
86 Thomas and Devasthale, 2014), nitrogen dioxide (NO₂; Pope et al., 2014) and particulate matter (i.e.

~~PM_{2.5}; Graham et al., 2020) to hazardous levels. Secondly, higher temperatures during blocking events, which can trap and accumulate existing pollutants (e.g. Pope et al., 2016), can lead to the secondary formation of tropospheric ozone (O₃). Elevated surface O₃ is associated with adverse health impacts (Doherty et al., 2017; Jerrett et al., 2009) with ailments such as asthma, reduced lung function and disease (WHO, 2021). It also has adverse impacts on the natural biosphere (Sitch et al., 2007) and agriculture (Hollaway et al., 2012; van Dingenen et al., 2009).~~

In this study, we use surface and satellite observations of O₃, in combination with the well-evaluated TOMCAT global chemical transport model (CTM), to investigate the impact of the summer 2018 heatwave on European AQ and determine the key processes driving observed surface/tropospheric O₃ enhancements. We describe the observations and model we have used in Section 2. Section 3 and Section 4 discusses our results and discussion/conclusions, respectively.

2. Observations and Model

2.1. Satellite and Surface Observations

We use satellite observations of lower tropospheric O₃ (i.e. sub-column O₃ (SCO₃) between the surface and 450 hPa) from the Global Ozone Monitoring Experiment (GOME-2) and the Infrared Atmospheric Sounding Interferometer (IASI) instruments on-board ESA's MetOp-A satellite, which was launched in 2006 into a sun-synchronous polar orbit with equator crossing times of 9:30 (day) and 21:30 (night). GOME-2 is a nadir-viewing spectrometer with spectral coverage in the ultraviolet-visible (UV-Vis) of 240–790 nm (Riese et al., 2012) and a ground footprint of 40 km × 80 km in the first part of the mission and 40 km x 40 km from 2013 (once Metop-B was commissioned). IASI is a Michelson interferometer which observes the infrared spectral range 645 to 2760 cm⁻¹ with spectral sampling of 0.25 cm⁻¹ (Illingworth et al., 2011). It measures simultaneously in four fields of view (circular at nadir with a diameter of 12 km) which are scanned across track to sample a 2200 km-wide swath (Clerbaux et al., 2009).

For GOME-2, the Rutherford Appleton Laboratory (RAL) scheme uses an optimal estimation algorithm (Rodgers, 2000) to retrieve ~~ozone~~ height-resolved ozone distributions spanning the stratosphere and troposphere (Miles et al., 2015). The scheme applied to GOME-2 has been developed from that used first for GOME-1 on-board ERS-2 (Munro et al., 1998; Forster et al., 2007). This is a multi-step scheme in which profile information is first retrieved in the stratosphere by exploiting wavelength-dependent absorption in the O₃ Hartley band (270-307nm) and is then extended into the troposphere by exploiting temperature-dependent spectral structure in the O₃ Huggins bands (325-335nm). For IASI, O₃ profiles are retrieved using an extended version of RAL's Infrared-Microwave-Sounding (IMS) scheme, which is described in Pope et al., (2021) ~~and~~ Palmer et al., (2022) ~~and Pimlott et al., (2022)~~. The IMS core scheme was originally developed to retrieve temperature, water vapour and stratospheric O₃ profiles along with surface spectral emissivity and cloud jointly from co-located measurements by IASI, the Microwave Humidity Sounder (MHS) and the Advanced Microwave Sounding Unit (AMSU-A) on MetOp (RAL Space, 2015). GOME-2 ~~and IMS~~ O₃ data were filtered for a geometric cloud fraction less than 0.2, a solar zenith angle less than 80°, a cost function less than 200.0 and a convergence flag equal to 1.0. ~~IASI data were filtered for a geometric cloud fraction less than 0.2 and a cost function less than 1000.0. Examples of the vertical sensitivity to retrieving ozone (i.e. averaging kernels) from GOME-2 and IMS are shown in~~ Supplementary Material (SM) 1.

129 We also use surface O₃ observations from the European Monitoring and Evaluation Programme
130 (EMEP) network for May-August 2017 and 2018. The EMEP network contains >100 surface
131 measurement sites measuring information on a range of air pollutions (e.g. ozone, NO₂ and PM_{2.5}).
132 EMEP surface data can be used for multiple scientific applications such as trends analysis (Yan et al.,
133 2018) and atmospheric chemistry model evaluation (Schultz et al., 2017; Archibald et al., 2020) and
134 is hosted by the EBAS database infrastructure, developed by the Norwegian Institute for Air
135 Research. In total, we used 125 spatial collocated EMEP sites in both years across Europe. Here, data
136 at individual sites were selected where the corresponding data flag was set to 0.0.~~We also use~~
137 ~~surface O₃ observations from the European Monitoring and Evaluation Programme (EMEP) network~~
138 ~~for May-August 2017 and 2018. In total, we used 83 spatial collocated EMEP sites in both years~~
139 ~~across Europe. Here, data at individual sites were selected where the corresponding data flag was~~
140 ~~set to 0.0.~~

141 2.2. Modelling & Sensitivity Experiments

142 In this study the TOMCAT CTM (Chipperfield, 2006) is forced by European Centre for Medium-Range
143 Weather Forecasts (ECMWF) ERA-Interim reanalysis meteorology (Dee et al., 2011) and is run at a
144 horizontal resolution of 2.8° × 2.8°. The model has with 31 vertical levels from the surface to 10 hPa
145 with 5-7 (approximately 10) levels in the boundary layer (mid-troposphere), depending on latitude.
146 ~~In this study the TOMCAT CTM (Chipperfield, 2006) is forced by European Centre for Medium-Range~~
147 ~~Weather Forecasts (ECMWF) ERA-Interim reanalysis meteorology (Dee et al., 2011) and run at a~~
148 ~~horizontal resolution of 2.8° × 2.8° with 31 vertical levels from the surface to 10 hPa.~~ The model
149 includes detailed tropospheric chemistry, including 229 gas-phase reactions and 82 advected tracers
150 (Monks et al., 2017), and heterogeneous chemistry driven by size-resolved aerosol from the
151 GLOMAP module (Mann et al., 2010). Anthropogenic emissions used in this study come from
152 MACCity (Granier et al., 2011). The original dataset in Granier et al., (2011) derived emissions up to
153 2010. Therefore, the Representative Concentration Pathways 8.5 (RCP 8.5) were used by Granier et
154 al., (2011) to generate emissions for later years (e.g. 2017 and 2018 as used in this study).
155 ~~Simulations used here include year-specific anthropogenic emissions from MACCity (Granier et al.,~~
156 ~~2011) and fire emissions from the Global Fire Assimilation System (GFAS, Kaiser et al., 2012) for~~
157 ~~2017 and 2018.~~ Year-specific off-line biogenic volatile organic compounds (VOCs) emissions for
158 acetone, methanol, isoprene and monoterpenes were simulated by the Joint UK Land Environment
159 Simulator (JULES – Pacifico et al., 2011; Best et al., 2011; Clark et al., 2011). All other biogenic VOC
160 emissions are climatological values and provided by the Chemistry-Climate Model Initiative (CCMI)
161 (Morgenstern et al., 2017). The global budgets of the JULES VOC emissions are low in comparison to
162 the climatological CCMI emissions, so were scaled up on a regional basis, while retaining the 2017-
163 2018 step change related to the 2018 summer heat wave. The full details of JULES VOC emissions
164 scaling can be found in Supplementary Material (SM) 34. Lightning emissions of NO_x are coupled to
165 convection in the model, which is derived from the meteorological reanalyses. Therefore, they vary
166 in space and time according to the seasonality and spatial pattern of convective activity (Stockwell et
167 al., 1999). The model was run for 2017 and 2018 with output at 6-hourly intervals (i.e. 00, 06, 12 and
168 18 UTC). Here, each year was run with its respective meteorology and emissions and given the labels
169 Met17_Emis17 (representing 2017) and Met18_Emis18 (representing 2018).

170 To explore the importance of emission and meteorological processes behind the elevated European
171 summer 2018 tropospheric O₃ levels, a 1-year model sensitivity experiment was performed using
172 2018 meteorology but 2017 emissions (i.e. Met18_Emis17). Therefore, the difference between

173 Met18_Emis17 and Met17_Emis17 highlights the impact of fixed emissions (i.e. 2017 emissions for
174 both years), while the Met18_Emis18 minus Met18_Emis17 highlights the impact of fixed
175 meteorology (i.e. 2018 meteorology for both years – including BVOC emissions). These are
176 compared with the control differences for 2018-2017 (Met18_Emis18- Met17_Emis17). From here
177 on in, we refer to the control differences, fixed emission differences and the fixed meteorology
178 differences as CTL_DIFF, FIXED_EMIS_DIFF and FIXED_MET_DIFF, respectively. TOMCAT also
179 includes a stratospheric O₃ tracer, a common approach to tag stratospheric O₃ (e.g. Roelofs et al.,
180 2003; Akritidis et al., 2019), which can be used to investigate the impact of stratospheric O₃ intrusion
181 into the troposphere. The tracer is set equal to the model-calculated O₃ in the stratosphere. The only
182 tropospheric source of O_{3s} is transport from the stratosphere while its sinks are via photolysis,
183 reactions with HO₂, OH and H₂O through O(¹D) produced from O_{3s} and surface deposition (Monks et
184 al., 2017). The tracer does not have a fixed lifetime but the loss rate in the troposphere depends on
185 the modelled local OH, HO₂, H₂O and photolysis. Any O₃ that gets into the stratosphere will be
186 labelled as stratospheric before it returns. TOMCAT also includes a stratospheric O₃-tracer (i.e. tags
187 O₃ in the model which originated in the stratosphere). This was used to investigate the impact of
188 stratospheric O₃ intrusion into the troposphere.

189 TOMCAT has been used in a number of previous studies to investigate air quality and tropospheric
190 composition (e.g. Richards et al., 2013; Emmons et al., 2015; ~~Pope et al., 2016~~; Pope et al., 2018;
191 Pope et al., 2020) whose results give confidence in the model's ability to simulate European
192 tropospheric O₃ in this study. Overall, when compared with observations, TOMCAT has good spatial
193 agreement with both GOME-2 and IASI and can reasonably reproduce the 2018 SCO₃ enhancement
194 in 2018 ~~verses-versus~~ 2017 (**SM 45**). The model also has good agreement, both in magnitude and
195 seasonality, with the EMEP observed surface concentrations (**SM 45**).

196 **2.3 ROTRAJ Back-trajectories**

197 We use the Reading Offline Trajectory Model (ROTRAJ) to generate air mass back-trajectories
198 (Methven et al., 2003) to assess the import of tropospheric O₃ into Europe. ROTRAJ is a Lagrangian
199 atmospheric transport model driven by meteorology from the same ECMWF ERA-Interim reanalyses
200 (horizontal resolution of 1.0125°) as used by TOMCAT. ROTRAJ is a Lagrangian atmospheric transport
201 model driven by meteorology from the same ECMWF ERA-Interim reanalyses as used by TOMCAT.
202 Velocity fields at the Lagrangian particle positions are determined by cubic Lagrange interpolation in
203 the vertical, bilinear interpolation in the horizontal and linear interpolation in time. This method
204 accounts for large scale advection since the winds are resolved but does not resolve small scale sub-
205 grid turbulent transport. Kinematic back-trajectories were released at 6-hourly intervals (i.e. at 00,
206 06, 12 and 18 UTC) from Paris and Berlin, both central locations over Europe in the region of
207 summer-time 2018 O₃ enhancements, between the 1st May and 31st August for both 2017 and 2018.
208 The trajectories were ~~released~~ at the surface and at approximately 500 hPa and integrated for 10
209 days with 6-hourly output (i.e. 41 trajectory points including the starting location) to investigate the
210 origin of air masses arriving in these altitude regions of enhanced summer-time O₃ in 2018. In total,
211 ROTRAJ was therefore run 8 times (2 years × 2 altitudes × 2 locations).

212 To quantify the import of tropospheric O₃ into Europe, for each trajectory, all the trajectory points
213 were co-located with corresponding TOMCAT O₃ mixing ratio values (i.e. the horizontal and vertical
214 grid box the trajectory point sits within and corresponding time stamp) and then the average O₃-
215 weighted back-trajectory (O₃-WBT) determined (i.e. back-trajectories with larger O₃WBT values

216 come from air masses with larger O₃ content). This follows a similar approach to Graham et al.,
217 (2020) and Stirling et al., (2020), though using a model chemical tracer and not emission inventories.

218 3. Results

219 3.1 Surface Temperature

220 Several studies (e.g. Li et al., 2020; Liu et al., 2020; Drouard et al., 2020) have documented the
221 intense heat wave across Europe in the summer of 2018. This is further shown in **Figure 1** which
222 compares surface temperature, co-retrieved with ozone and other variables from MetOp-A by the
223 IMS scheme, between 2017 and 2018. In May, higher temperatures occur across Scandinavia (5.0-
224 10.0 K), eastern Europe (3.0-7.0 K) and the UK (1.0-3.0 K), but temperatures are lower (-3.0 to -1.0 K)
225 across Iberia. In June, a similar spatial distribution occurs but the magnitude of the differences is
226 smaller. In July the largest temperature increases range from 6.0-8.0 K in Scandinavia to 2.0-6.0 K in
227 the UK/France. Iberia continued to experience temperatures lower by -2.0 to 0.0 K. In August, there
228 are near-zero differences over the UK, Iberia and most of Scandinavia but with increases of 1.0-3.0 K
229 over eastern Europe and Finland.

230 3.2 Satellite Ozone

231 We investigate the longer term variability in tropospheric O₃ (i.e. SCO₃) to determine if 2017 is a
232 suitable comparator for the 2018 summer O₃ enhancements as it is for temperature. **Figure 2** shows
233 the 2012-18 SCO₃ average between May and August for a domain over the Atlantic and Europe and
234 the difference for the same season between specific years and the 2012-18 average. In 2012 and
235 2013, there are significant positive differences from the average between 1.0 DU and 5.0 DU over
236 much of the domain. Over continental Europe, the differences are smaller. Here, the significance of
237 differences between the year-specific and long-term averages are determined using the Wilcoxon
238 Rank test (Pirovano et al., 2012) at the 95% confidence level. In 2014 and 2015, there are negative
239 differences across Europe (-4.0 DU to -1.0 DU). In 2016, similar negative differences are primarily
240 across the north and south-east of the domain. In 2017, there are near-zero differences across the
241 Atlantic, UK and western Europe. Over eastern Europe and Mediterranean, there are significant
242 negative differences of between -2.0 DU and -1.0 DU. In 2018, across continental Europe there are
243 significant positive differences between 2.0 DU and 4.0 DU. As the 2017 differences are relatively
244 small in magnitude with a low proportion of significant pixels (i.e. Sig Pixels % = 32.7 is the lowest
245 across the 7 years), it is representative of average conditions for comparison with 2018. For 2018,
246 the summer SCO₃ enhancements across continental Europe are the largest for the years shown with
247 a coherent cluster of significant differences. This illustrates that the summer 2018 SCO₃
248 enhancements are a substantial deviation from the average conditions (which we represent as 2017
249 hereon) and that this is an intense O₃ event.

250 Investigation of SCO₃ retrieved from both GOME-2 (**Figure 3**) and the IMS scheme (**Figure 4**) show
251 consistent enhancements in summer 2018. In 2017, between May and August, GOME-2 typically
252 observed SCO₃ values between 20.0-30.0 DU across continental Europe. Peak SCO₃ values occurred
253 over the Mediterranean (30.0-38.0 DU); relatively high ozone is a typical feature of the
254 Mediterranean in summer (Richards et al., 2013). In 2018, the seasonality is consistent with 2017,
255 but the continental European SCO₃ values ranged between 25.0 DU and 35.0 DU. For the 2018-2017
256 difference, SCO₃ enhancements occur across continental Europe in all four ~~months, but~~ months but
257 peaked in May and July between 3.0 DU and 8.0 DU, while typically 1.0-5.0 DU in June and August.

258 The spatial distribution of IMS-retrieved SCO_3 is similar to that of GOME-2 in 2017 and 2018,
259 although the absolute values tend to be systematically lower by 3.0-4.0 DU. However, despite this
260 systematic offset, the 2018-2017 differences are reasonably consistent with GOME-2. Across
261 continental Europe, IMS SCO_3 shows 2018 enhancements in all months investigated, but peaks in
262 May and July, like GOME-2, between 3.0 DU and 6.0 DU. The differences range from 1.0 DU to 3.0
263 DU in June and are approximately 1.0 DU in August (though a peak enhancement of 3.0-5.0 DU
264 occurs over the Mediterranean). Spatial correlations between the GOME-2 and IASI difference (i.e.
265 2018-2017) maps for the months investigated ranged between 0.21 and 0.47 (see **SM 45**).

266 The GOME-2 and IASI instruments observe UV-Vis and IR wavelengths, with peak vertical sensitivities
267 to tropospheric O_3 in the lower and mid/upper troposphere, respectively. Consistency in the 2018
268 enhancements in SCO_3 indicates that these extend over the bulk of the troposphere and increases
269 confidence in the differences for both sensors.

270 Investigation of several satellite-retrieved O_3 precursor gases (see **SM 12**) showed enhancements in
271 total column methanol (TCCH_3OH , **Figure S1S2**), especially linked to May and July temperature
272 enhancements (**Figure 1**), minor increases in tropospheric column NO_2 (TCNO_2 , **Figure S2**) in May and
273 July over central Europe and widespread enhancements (weakest in July and strongest in August) in
274 total column carbon monoxide (TCCO , **Figure S3S4**). Investigation of the GOME-2 and IASI total
275 column O_3 (TCO_3) differences between 2017 and 2018 (**Figures S4-S5 & S5S6**) showed these to be in
276 close agreement. Some spatial structure is similar to that of the SCO_3 difference patterns (**Figures 3**
277 **and 4**), with correlations of approximately 0.5 between TCO_3 and SCO_3 for each instrument (see **SM**
278 **23**). Given the complex relationship between tropospheric O_3 , precursor gases, atmospheric
279 chemistry (e.g. NO_x or VOC-limited regimes), surface deposition and meteorological conditions (e.g.
280 atmospheric temperatures and transport), a detailed chemistry transport model is required to assess
281 the key processes leading to the observed SCO_3 enhancements over Europe.

282 3.3 Surface Ozone

283 Increased temperatures during heat waves have been shown to enhance surface O_3 concentrations
284 (e.g. Jacob and Daniel, 2009; Vieno et al., 2010; Pyrgou et al., 2018). In the summer (May-June-July-
285 August, MJJA) of 2018, EMEP recorded larger O_3 mixing ratios across most of Europe in comparisons
286 to 2017 (**Figure 5a & b**). Over central Europe, surface O_3 mixing ratios ranged from approximately
287 45.0 ppbv to over 60.0 ppbv, while in 2017 it was 35.0 ppbv to 50.0 ppbv. Over the UK and north-
288 western Europe, surface O_3 mixing ratios ranged from 20.0 ppbv to 30.0 ppbv and then 25.0 ppbv to
289 35.0 ppbv in MJJA 2017 and 2018, respectively. In Scandinavia and eastern Europe, surface O_3 mixing
290 ratios ranged from 20.0 ppbv to 35.0 ppbv in MJJA 2017, while increasing to 25.0 ppbv to
291 approximately 40.0 ppbv in MJJA 2018. **Figure 5c** highlights these widespread enhancements where
292 domain-average surface O_3 mixing ratios are larger by typically 5.0-10.0 ppbv in May and from mid-
293 June to mid-August in 2018. **Figure 5d** shows that the domain median surface O_3 concentration
294 across MJJA was larger by 2.0-3.0 ppbv in 2018, but the 2018 extremes were greater with 75th and
295 95th percentiles of 4245.0 ppbv and 5355.0 ppbv in 2017 and 4748.0 ppbv and 59.0 ppbv in 2018.
296 Therefore, surface observations of O_3 recorded widespread enhancements in MJJA 2018 compared
297 to 2017 with peak site differences >10.0 ppbv. This is generally consistent with the 2018 layer-
298 averaged enhancements in the satellite-retrieved SCO_3 for regions where both datasets have spatial
299 coverage.

300 3.4. Model Simulations

301 We use the TOMCAT model to investigate different factors potentially driving the observed
302 enhancements in tropospheric O₃. In comparisons with the observations (see **SM 45**) the model
303 reproduces the sign and spatial distribution of observed 2018-2017 differences reasonably well.
304 Although it has a tendency to underestimate the absolute magnitude, we are confident in the
305 model's ability to simulate the tropospheric O₃ enhancements relative to 2017.

306 At the surface (**Figure 6**), TOMCAT CTL_DIFF (i.e. Met18_Emis18 - Met17_Emis17) suggests that O₃ is
307 enhanced in May over Scandinavia (2.0- >5.0 ppbv), north-western Europe (0.0-2.0 ppbv), the Arctic
308 Ocean (>5.0 ppbv) and off the coast of Iberia (3.0-5.0 ppbv). However, negative values exist over
309 eastern Europe (-3.0 ppbv to -1.0 ppb) and the Atlantic west of Ireland (-3.0 ppbv to -1.0 ppb). In
310 June, the negative differences persist in eastern Europe (-3.0 ppbv to -1.0 ppb), but positive
311 differences are located over northern Scandinavia (1.0-2.0 ppbv) and the North Atlantic (2.0-4.0
312 ppbv). For July, CTL_DIFF shows the largest enhancements over continental Europe (i.e. Po Valley,
313 France, Benelux region and Iberia) and the UK (>5.0 ppbv). Negative differences of between -3.0
314 ppbv and -1.0 ppbv remain over eastern Europe. In August, the only clear differences are over Iberia
315 and the western Mediterranean, ranging between 3.0 ppbv and >5.0 ppbv. Overall, TOMCAT
316 simulates sub-regional surface O₃ enhancements over Europe, which are generally consistent with
317 EMEP observations apart from several sites over eastern Europe.

318 At 500 hPa, TOMCAT CTL_DIFF shows larger-scale O₃ enhancements in 2018 compared to 2017 (>5.0
319 ppbv) throughout May to August. In May and August, there are, however, a few negative differences
320 (-5.0 ppbv to -3.0 ppbv) over far eastern Europe. In June and July, the full domain is more or less
321 dominated by O₃ enhancements in 2018. In Figures 4 and 5 (and **SM 45**), GOME-2 and IASI (and
322 TOMCAT with the instrument averaging kernels (AKs) applied to account for the vertical sensitivity of
323 the retrievals, see **SM 4-5** for more information) show SCO₃ enhancements during these months of
324 2018. Given the vertical extents and peak heights of their retrieval sensitivities and consistency in
325 spatial patterns (**Figs SM-8 and 10**) it is evident that the O₃ enhancements detected by GOME-2 and
326 IASI extend over the free troposphere. The model shows large-scale O₃ enhancements in the free
327 troposphere and similar patterns to GOME-2 and IASI when averaging kernels applied. So the model
328 corroborates this finding from the satellite retrievals. Signals from EMEP and TOMCAT at the surface,
329 on the other hand, are more mixed across the domain.

330 The right-hand column of **Figure 6** shows the relative difference in the stratospheric O₃ contribution
331 to the 500 hPa O₃ layer (i.e. Strat % @ 500 hPa), from CTL_DIFF, between 2017 and 2018. Here, the
332 percentage of stratospheric O₃ contributing to the O₃ concentration at the 500 hPa is calculated for
333 2017 and 2018 and then the 2018-2017 difference determined. The largest enhancement to the 500
334 hPa layer was in July where the stratospheric O₃ contribution increased by 3.0% to >5.0% across
335 Europe. In June and August, the spatial patterns are similar with stratospheric O₃ contribution
336 enhancements of 3.0-5.0% across southern Europe, Scandinavia and the North Atlantic (above the
337 UK). In the North Atlantic, UK and northern Europe, there are near-zero changes in June and August.
338 In May, there are enhancements >5.0% across the northern region of the domain and northern
339 Africa, while smaller enhancements (1.0%-3.0%) over the UK and near-zero changes over eastern
340 Europe. This is partially supported by analysis of TCO₃ (see **SM 23**) where there are reasonable
341 spatial correlations (~0.5 to 0.6) between the SCO₃ 2017-2018 summer differences and the
342 equivalent for TCO₃. Therefore, these results indicate a potentially enhanced contribution of
343 stratospheric O₃ into the mid-troposphere during the summer of 2018 across Europe.

344 To quantify the separate importance of precursor emissions and meteorology in governing the
345 summer 2018 O₃ enhancements we compare the sensitivity experiments with the control runs.
346 **Figure 7** (left column) shows the results for the fixed emissions differences (i.e. FIXED_EMIS_DIFF)
347 between years (i.e. Met18_Emis17 – Met17_Emis17). At the surface, the FIXED_EMIS_DIFF show
348 similar spatial patterns to that of CTL_DIFF (**Figure 6** – left column). The domain spatial difference
349 correlations between these simulations is greater than 0.96 for all months considered. However,
350 FIXED_EMIS_DIFF (**Figure 7** - left column) tends to be lower than CTL_DIFF (**Figure 6** – left column)
351 by approximately 0.0-2.9 ppbv (i.e. positive red regions are weaker and negative blue regions
352 stronger in intensity). Therefore, the Met18_Emis17 run struggles to reproduce the absolute surface
353 O₃ enhancements in the Met18_Emis18 run. When the fixed meteorology differences
354 (FIXED_MET_DIFF, i.e. Met18_Emis18 - Met18_Emis17, **Figure 8** - left column) are compared with
355 CTL_DIFF, the surface 2018-2017 differences are substantially different.

356 Surface FIXED_MET_DIFF ranges between 0.0 ppbv and 2.0 ppbv across the domain in May and June
357 and is more confined to continental Europe in July and August. This shows that TOMCAT simulates
358 lower 2018 summer-time O₃ when 2017 emissions are used and indicates that emissions do have
359 some role in controlling O₃ levels at the surface. However, as the spatial difference pattern for
360 FIXED_MET_DIFF (**Figure 8** – left column) is different to that of CTL_DIFF (**Figure 6** – left column),
361 spatial correlations between them range from -0.53 to 0.54 over the four months, it suggests that
362 meteorology is important in governing the spatial distribution of CTL_DIFF. This is supported by the
363 fact that FIXED_MET_DIFF - CTL_DIFF (**Figure 8** left column – **Figure 6** left column) yields absolute
364 domain variations between 0.0 ppbv and 12.2 ppbv. Therefore, the two sensitivity experiments
365 suggest meteorology and emissions both play important roles in controlling surface O₃ during the
366 summer of 2018, but meteorology predominantly governs the spatial pattern and absolute
367 magnitude of the O₃ enhancements.

368 At 500 hPa, comparison of FIXED_EMIS_DIFF and CTL_DIFF show very consistent spatial patterns
369 across the four months with correlations all above 0.98. In terms of the absolute differences
370 between FIXED_EMIS_DIFF and CTL_DIFF (i.e. **Figure 7** centre column – **Figure 6** centre column) it
371 peaks at approximately 2.8 ppbv. For FIXED_MET_DIFF, the spatial correlation with CTL_DIFF, as for
372 the surface, is variable with values between -0.38 and 0.43. The absolute differences between
373 FIXED_MET_DIFF and CTL_DIFF (i.e. **Figure 8** centre column – **Figure 6** centre column) ranges from
374 0.0 ppbv to 14.8 ppbv. Therefore, emissions have a secondary role in controlling the O₃ while
375 meteorology is by far the dominant factor. For Strat % @ 500 hPa, the spatial correlations between
376 CTL_DIFF and FIXED_EMIS_DIFF are above 0.95 for all months and the absolute differences between
377 them (i.e. **Figure 7** right column - **Figure 6** right column) are near-zero. Comparison of
378 FIXED_MET_DIFF and TC_CTL shows spatial difference correlations ranging between -0.33 and 0.71
379 and absolute differences (i.e. **Figure 8** right column - **Figure 6** right column) peaking at 12.9%.
380 Therefore, as expected, meteorological processes are dominating the influence of the stratospheric
381 O₃ contribution (i.e. through stratosphere-troposphere exchanges) to the 500 hPa layer during the
382 summer 2018 O₃ enhancements over Europe.

383 To investigate the importance of stratospheric-troposphere exchange to the middle troposphere
384 enhancement (i.e. as shown in the TOMCAT 500 hPa layer and the satellite SCO₃ data), **Figures 9** and
385 **10** show TOMCAT control run zonal 2018-2017 difference cross-sections (for the domain longitudes)
386 of O₃ profiles and the stratospheric O₃ contribution to each pressure layer. In May and June, in the
387 lower troposphere (approximately surface to 800 hPa), there are negative (-3.0% to 0.0%) and

388 positive (0.0% to 3.0%) differences between 30-50°N and 50-70°N, respectively. During June, there
389 are positive differences (0.0% to 5.0%) across most latitudes and in August, the opposite occurs to
390 that of May/June. In the mid-troposphere (800-300 hPa), positive differences occur in most months
391 (0.0-5.0% in May, 0.0-7.0% in June, >10% in July and 5.0-10.0% in August), though in May and August
392 negative differences (-5.0% to 0.0%) exist around 40°N and 55°N. This is consistent with the 500 hPa
393 O₃ differences in **Figure 6** (centre panels). In the upper troposphere – lower stratosphere (UTLS,
394 approximately 300-100 hPa) there are limbs of positive O₃ differences (i.e. >10%, 5.0-10.0 ppbv)
395 propagating into the mid-troposphere (30-40°N in May, 30-50°N in June, 40-50°N in July and 30-40°N
396 & 60-70°N in August), suggestive of stratospheric intrusion into the mid-troposphere. Using the
397 stratospheric O₃ tracer in TOMCAT, **Figure 10** shows the enhanced proportion of O₃ originating from
398 the stratosphere in the summer of 2018. Interestingly, for all months (apart from May between 30-
399 45°N), there are enhanced contributions of stratospheric O₃ (15.0% to >50.0%) in the lower-mid
400 troposphere (i.e. below 500 hPa). In absolute terms, this is only a minor contribution typically below
401 800 of <1.0 ppbv. Between 800-400 hPa, this increases to 1.0-5.0 ppbv (remains relatively consistent
402 in percentage terms) in most months and latitude bands. In the UTLS, it increases to 5.0-10.0%
403 enhancements in stratospheric O₃ contributions, which is consistent with its proximity to the
404 stratosphere. In comparison between **Figures 9** and **10**, where there are enhancements in the
405 stratospheric O₃ contribution but negative differences in O₃ (e.g. in June in the lower troposphere
406 between 50°N and 55°N) which is suggestive of different processes influencing the O₃ concentrations
407 (e.g. descent of relatively small stratospheric O₃ contributions but advection of tropospheric O₃ away
408 from the region). Overall though, in the mid-troposphere, where there are larger enhancements in
409 O₃, there are similar responses in the stratospheric O₃ contribution. For June, the mid-troposphere
410 O₃ enhancement is approximately 5.0-7.0 ppbv with a signal of 1.0-2.0 ppbv in the stratospheric
411 tracer. Therefore, in the more extreme cases, the stratospheric O₃ contribution is approximately
412 15.0-40.0% to the mid-tropospheric O₃ enhancements in summer 2018 over Europe. However, a
413 separate study would be required to undertake a detailed assessment of the meteorological
414 processes controlling the enhanced stratospheric intrusion of ozone in the summer of 2018 and how
415 it compares to other years (how does it compare with other years other than 2017).

416 The two remaining factors, linked to meteorological processes (as suggested above), which may
417 affect the O₃ enhancements in 2018 are increased summer temperatures (e.g. through enhanced
418 kinetic rates), and the import of tropospheric O₃ from upwind (e.g. North America from the
419 prevailing winds). **Figure 11** shows the 2017-2018 zonal temperature differences (i.e. same as **Figure**
420 **9** but for temperature) with the correlation between the 2017 and 2018 temperature and O₃
421 differences overplotted. Qualitatively, the zonal differences in O₃ and temperature have some
422 similarities. There are positive differences (temperature differences of 0.0-1.0%) between 50-60°N
423 and the surface and 400 hPa in May and June. Then in July, collocated positive differences (peaking
424 at 2.0% or 3.0 K) exist between 50-70°N from the surface to 300 hPa. In August, there is no clear
425 relationship between temperature and O₃ enhancements. In all months (to a lesser extent in
426 August), in the UTLS, there are spatial agreements with positive differences between approximately
427 30-45°N and negative differences between 50/55-70°N. In terms of correlations (i.e. temporal
428 correlation in each grid box using the TOMCAT 6-hourly time series), the spatial agreement is
429 relatively weak. In all months, most of domain has relatively small values ranging between -0.5 to
430 0.5. There are only a few locations with strong correlations (i.e. > 0.5), which are in the UTLS or in
431 the lower-mid troposphere between 50-70°N (June & August) and 45-55°N in July near the surface.

432 Overall, the relationship between increased temperatures and enhanced kinetic rates yielding more
433 ozone formation is non-linear, so it is unsurprising that the direct comparisons of temperature and
434 ozone 2018-2017 differences above shows no clear pattern. Therefore, future work could include a
435 further sensitivity experiment running TOMCAT for 2018, but with 2017 temperatures used in the
436 chemistry routines to quantify the role of temperature in the summer 2018 O₃ enhancements.

437 To investigate the potential advection of tropospheric O₃-rich air masses into Europe we have used
438 ROTRAJ back-trajectories to determine the O₃WBTs (i.e. an indicator of air mass O₃ content). As
439 shown in **SM_56**, there is large variability in the O₃WBT values and spatial distribution (i.e. **Figures**
440 **SM 12-13** and **1314**), so they have to be gridded onto the TOMCAT horizontal resolution (see **Figures**
441 **SM145** and **1516**). While this approach does not directly account for the frequency of trajectory
442 points in each grid box, **Figures SM 13 and 14** show there is widespread coverage across the North
443 Atlantic. This results in >500 trajectory points near the receptor sites (i.e. Paris and Berlin), ~100
444 trajectory points around the edge of Europe and 25-50 trajectory points in the North Atlantic (not
445 shown here). Overall, this spatial distribution is relatively consistent and does not change
446 substantially between years (typically 10%), thus this approach is suitable in this study. **Figure 12**
447 shows the differences (2018-2017) between the gridded O₃WBTs where the back-trajectories have
448 been released at the surface from Paris (**Figure 12a**), at the surface from Berlin (**Figure 12b**), at
449 approximately 500 hPa from Paris (**Figure 12c**) and at approximately 500 hPa from Berlin (**Figure**
450 **12d**). We selected Paris and Berlin as they are situated in central Europe where the summer 2018 O₃
451 enhancements have been observed while the surface and 500 hPa are the altitudes of primary focus
452 in the modelling work.

453 At the surface, Paris and Berlin show consistent patterns. Over the North Atlantic (i.e. origin of the
454 prevailing winds into Europe), there are typically negative O₃WBT values between -5.0 ppbv and -1.0
455 ppbv suggesting that advection of O₃ into Europe during the summer (i.e. May-August) was
456 predominantly larger in 2017 and did not strongly contribute to the 2018 -observed surface O₃
457 enhancements. Advection of O₃-rich air in 2018 did originate from Scandinavia into continental
458 Europe, though the number of trajectories is relative low (see **Figure S12**). As both locations show
459 similar relationships, it provides confidence in this methodology. At 500 hPa, the 50-60°N spatial
460 pattern is less defined with values typically between -5.0 and 5.0 ppbv for both locations. However,
461 in the southern North Atlantic (30-50°N) there are positive differences of approximately 3.0-10.0
462 ppbv for both release locations. Note that as free-tropospheric winds tend to have larger horizontal
463 velocities, the back-trajectories generally start from further away closer to North America. Again,
464 given the broad similarity in differences between both release locations, it provides confidence in
465 this approach. Overall, our results indicate a larger transport of O₃ to the surface of continental
466 Europe in 2017, while at approximately 500 hPa the import of O₃ into Europe is larger in 2018. Here,
467 the positive differences originate from the southern North Atlantic (i.e. a larger range of locations,
468 absolute values and homogeneous signal than the mixed differences between 50-60°N).

469 One potentially important factor is dry deposition of O₃ to the land surface. Due to the heatwave,
470 stress on the biosphere and the associated die back of vegetation could potentially reduce the
471 efficiency of O₃ deposition decreasing the O₃ sink (i.e. O₃ is more likely to deposit onto land covered
472 by vegetation than bare soil). Investigation of the normalised difference vegetation index (NDVI),
473 from the IMS scheme, between the summers of 2017 and 2018 did not highlight any spatially
474 coherent changes (not shown here). As a result, there is no obvious large-scale spatial vegetation die
475 back in 2018 due to the heatwave and thus the impact this would have on ozone deposition in

476 TOMCAT. Therefore, we ran two further experiments where the bare soil fraction for each grid box
477 over Europe was increased and decreased by 25% in summer 2018. This was to investigate the
478 sensitivity of surface ozone deposition to changes in the land surface. For the increase in bare soil
479 fraction there was a moderate systematic increase in European summer ozone by 0.0-1.5 ppbv (i.e.
480 less ozone deposition). When the bare soil fraction was decreased by 25%, this yielded a small
481 decrease in surface ozone by approximately 0.5 ppbv. Overall, a sizable level of vegetation die back
482 would be required for decreased ozone dry deposition to substantially contribute to the summer
483 2018 surface ozone enhancements.

484 **4. Discussion and Conclusions**

485 The summer of 2018 produced an intense heatwave across most of Europe with a substantial impact
486 on tropospheric temperatures, droughts, stress on vegetation and human mortality. Observations of
487 surface temperature, precursor gases and total column O₃ (TCO₃) experienced enhancements in
488 2018 relative to 2017. In this paper we have demonstrated a strong enhancement in surface and
489 tropospheric O₃ during the heatwave between May and August 2018. The EMEP surface data
490 suggest an average European enhancement, relative to 2017, peaking at approximately 10.0 ppbv in
491 July and August. Investigation of lower tropospheric O₃ (i.e. surface-450 hPa sub-column O₃ – SCO₃)
492 from the GOME-2 and IASI instruments also showed enhancements, peaking at 5.0-10.0 DU, relative
493 to 2017. Analysis of the long-term GOME-2 SCO₃ record indicates 2017 to be a suitably
494 neutral/average reference year and the enhancement in 2018 to be anomalously large. Our
495 comparisons were therefore made between the summers of 2017 and 2018.

496 Consistency between the UV (GOME-2) and IR (IASI) sounders was important to our analysis because
497 their vertical sensitivities peak in the lower and mid-upper troposphere, respectively. The similar
498 patterns of SCO₃ enhancement detected by the two sounders therefore indicate that these extend
499 over the bulk of the troposphere, supportive of surface/lower tropospheric ozone enhancements.
500 This consistency also provides confidence that the complementary vertical sensitivities of GOME-2
501 and IASI ozone retrievals could be exploited in further investigation of tropospheric ozone (e.g. long-
502 term trends from multiple platforms/retrieval schemes has shown large-scale inconsistencies in
503 other studies e.g. Gaudel et al., (2018)) in the future.

504 Tropospheric O₃ behaviour is complex and the summer 2018 enhancements over Europe could
505 potentially have been caused by various factors: atmospheric chemistry, meteorology (e.g.
506 temperature, advection of O₃-rich air masses), anthropogenic and natural precursor emissions, dry
507 deposition and stratospheric intrusion. To investigate the interactions between these processes,
508 potentially leading to the summer 2018 O₃ enhancements, we used the well-evaluated TOMCAT 3D
509 CTM. Evaluation of the model in this study showed that it could accurately capture the spatial
510 pattern, temporal evolution and sign (i.e. positive 2018-2017 O₃ differences) of the O₃
511 enhancements and that, although it underestimated the observed enhancements, TOMCAT is an
512 adequate tool to investigate them.

513 The results of several model simulations showed that the surface ozone enhancements (mainly in
514 north-western Europe) in the summer of 2018 were predominantly driven by meteorological
515 processes with emissions acting as a secondary factor. As the ROTRAJ back-trajectories suggest that
516 advection of summer-time O₃ was larger in 2017, the 2018 European O₃ enhancements at surface
517 level were likely from in-situ processes. The TOMCAT stratospheric O₃ tracer indicated a negligible
518 contribution of stratospheric O₃ to these surface enhancements. At 500 hPa, the enhancement in

519 tropospheric O₃ is much larger spatially across Europe and dominated by meteorological processes.
520 Intrusion of stratospheric O₃ into the mid-troposphere has a moderate influence on the
521 observed/modelled O₃ enhancements with contributions of up to 15.0-40.0%. Correlations between
522 TOMCAT temperature and O₃ enhancements show broad agreement at some latitudes (e.g. 50-70°N
523 in the lower-mid troposphere). However, this relationship is non-linear and difficult to quantify
524 without further simulations/model tracers, which was beyond the scope of this study. ROTRAJ back-
525 trajectories suggest that in 2018, relative to 2017, there is the advection of more O₃-rich airmasses
526 into the European mid-troposphere contributing to the summer 2018 O₃ enhancements at this
527 altitude. Therefore, in the summer of 2018 over Europe, in-situ meteorological processes appear to
528 be predominantly driving surface O₃ enhancements over Europe, while advection of tropospheric O₃-
529 rich air and stratospheric intrusion are driving the corresponding tropospheric O₃.

530 Overall, through our study focusing on the European summer 2018 air pollution episode, we have
531 demonstrated the use of novel satellite datasets and a modelling framework (i.e. targeted sensitivity
532 experiments and model tracers) suitable to investigate the air quality impacts from future European
533 heatwaves such as that which occurred in summer 2022.

534 **Acknowledgements**

535 This work was funded by the UK Natural Environment Research Council (NERC) by providing funding
536 for the National Centre for Earth Observation (NCEO, award reference NE/R016518/1).

537 **Conflicting Interests**

538 The authors declare that they have no conflicts of interest.

539 **Date Availability**

540 The TOMCAT simulations are publically available at
541 http://homepages.see.leeds.ac.uk/~earrjpo/european_summer_2018_o3/tomcat, while the RAL
542 Space satellite can be found at
543 http://homepages.see.leeds.ac.uk/~earrjpo/european_summer_2018_o3/satellite. The EMEP
544 surface O₃ data was obtained from <http://ebas-data.nilu.no/default.aspx>. The GOME-2 tropospheric
545 column NO₂ data was downloaded from EUMETSAT at https://acsaf.org/nrt_access.php. The
546 TOMCAT and RAL Space satellite data will be uploaded to the Zenodo open access portal
547 (<https://zenodo.org/>) if this manuscript is accepted for publication in ACP after the peer-review
548 process.

549 **Author Contributions**

550 RJP, MPC and BJK conceptualised and planned the research study. RJP performed the TOMCAT
551 model simulations with support from MPC and WF. The JULES BVOC emissions were provided by ECP
552 and GDH. RJP analysed the satellite data provided by RAL Space (BJK, RS, BGL and LJV) with support
553 from BJK, RS and BGL. RJP undertook the EMEP analysis. RJP ran ROTRAJ with technical support from
554 SRA and AMG. RJP prepared the manuscript with contributions from all co-authors.

555 **References**

556 [Akritidis, D., Pozzer, A. and Zanis, P. 2019. On the impact of future climate change on tropopause](#)
557 [folds and tropospheric ozone. *Atmospheric Chemistry and Physics*, **19**, 14387-14401, doi:](#)
558 [10.5194/acp-19-14387-2019.](#)

559 [Archibald, A.T., et al. 2020. Description and evaluation of the UKCA stratosphere–troposphere](#)
560 [chemistry scheme \(StratTrop vn 1.0\) implemented in UKESM1. *Geoscientific Model Development*, 13,](#)
561 [1223–1266, doi: 10.5194/gmd-13-1223-2020.](#)

562 Bastos, A., Ciais, P., Friedlingstein, P., et al.: Direct and seasonal legacy effects of the 2018 heat wave
563 and drought on European ecosystem productivity, *Science Advances*, 6, eaba2724,
564 doi:10.1126/sciadv.aba2724, 2020.

565 Best, M.J., Pryor, M., Clark, D.B., et al.: The Joint UK Land Environment Simulator (JULES), model
566 description—Part 1: energy and water fluxes, *Geoscientific Model Development*, 4, 677–699,
567 doi:10.5194/gmd-4-677-2011, 2011.

568 Chipperfield, M.P.: New version of the TOMCAT/SLIMCAT off-line chemistry transport model:
569 Intercomparison of stratospheric trace experiments, *Quarterly Journal of the Royal Meteorological*
570 *Society*, 132, 1179–1203, doi:10.1256/qj.05.51, 2006.

571 [Churkina, G., Kuik, F., Bonn, B., et al. 2017. Effect of VOC Emissions from Vegetation on Air Quality in](#)
572 [Berlin during a Heatwave. *Environmental Science and Technology*, 51\(11\), 6120-6130, doi:](#)
573 [10.1021/acs.est.6b06514.](#)

574 Clark, D. B., Mercado, L.M., Sitch, S., et al.: The Joint UK Land Environment Simulator (JULES), model
575 description—Part 2: carbon fluxes and vegetation dynamics, *Geoscientific Model Development*, 4,
576 701–722, doi:10.5194/gmd-4-701-2011, 2011.

577 Clerbaux, C., Boynard, A., Clarisse, L., et al.: Monitoring of atmospheric composition using the
578 thermal infrared IASI/MetOp sounder, *Atmospheric Chemistry and Physics*, 9 (16), 6041–6054,
579 doi:10.5194/acp-9-6041-2009, 2009.

580 Dee, D.P., Uppala, S.M., Simmons, A.J., et al.: The ERA-Interim reanalysis: Configuration and
581 performance of the data assimilation system, *Quarterly Journal of the Royal Meteorological Society*,
582 137 (656), 553–597, doi:10.1002/qj.828, 2011.

583 Dirmeyer, P.A., Balsamo, G., Blyth, E.M., et al.: Land-Atmosphere Interactions Exacerbated the
584 Drought and Heatwave Over Northern Europe During Summer 2018, *AGU Advances*, 2,
585 e2020AV000283., doi: 10.1029/2020AV000283, 2020.

586 Doherty, R. M., Heal, M. R., and O'Connor, F. M.: Climate change impacts on human health over
587 Europe through its effect on air quality, *Environmental Health*, 16(1), 33–44, doi:10.1186/s12940-
588 017-0325-2, 2017.

589 Drouard, M., Kornhuber, K. and Woollings, T.: Disentangling Dynamical Contributions to Summer
590 2018 Anomalous Weather Over Europe, *Geophysical Research Letter*, 46, 12537-12546,
591 doi:10.1029/2019GL084601, 2020.

592 Emmons, L. K., Arnold, S. R., Monks, S. A., et al.: The POLARCAT Model Intercomparison Project
593 (POLMIP): overview and evaluation with observations, *Atmospheric Chemistry and Physics*, 15, 6721–
594 6744, doi:10.5194/acp-15-6721-2015, 2015.

595 Forster, P., Ramaswamy, V., Artaxo, P., et al.: Changes in Atmospheric Constituents and in Radiative
596 Forcing, in: *Climate Change 2007: The Physical Science Basis. Contribution of Working Group I to the*
597 *Fourth Assessment Report of the Intergovernmental Panel on Climate Change*, Cambridge University
598 Press, Cambridge, United Kingdom and New York, NY, USA, 2007.

599 [García-Herrera, R., Díaz, J., Trigo, R.M., et al. 2020. A Review of the European Summer Heat Wave of](#)
600 [2003. *Critical Reviews in Environmental Science and Technology*, 40\(4\), 267-](#)
601 [306, doi:10.1080/10643380802238137.](#)

602 Gaudel, A., Cooper, O.R., Ancellet, G., et al.: Tropospheric Ozone Assessment Report: Present day
603 distribution and trends of tropospheric ozone relevant to climate and global atmospheric chemistry
604 model evaluation. *Elementa*, 6(39), 1-58, doi:10.1525/elementa.291, 2018.

605 Graham, A. M., Pringle, K. J., Pope, R. J., et al.: Impact of the 2019/2020 Australian megafires on air
606 quality and health, *GeoHealth*, 5, e2021GH000454, doi:10.1029/2021GH000454, 2020.

607 Granier, C., Bessagnet, B., Bond, T., et al.: Evolution of anthropogenic and biomass burning emissions
608 of air pollutants at global and regional scales during the 1980–2010 period, *Climatic Change*, 109,
609 163-190, doi:10.1007/s10584-011-0154-1, 2011.

610 Guerreiro, S.B., Dawson, R.J., Kilsby, C., et al.: Future heat-waves, droughts and floods in 571
611 European cities, *Environmental Research Letters*, 13, 034009, 10.1088/1748-9326, 2018.

612 [Heal, M.R., Heaviside, C., Doherty, R.M., et al. 2013. Health burdens of surface ozone in the UK for a](#)
613 [range of future scenarios. *Environment International*, 61, 36-44, doi:10.1016/j.envint.2013.09.010.](#)

614 Hollaway, M.J., Arnold, S.R., Challinor, A. J. and Emberson, L.D: Intercontinental trans-boundary
615 contributions to ozone-induced crop yield losses in the North Hemisphere, *Biogeosciences*, 9, 271–
616 2929, doi: 10.5194/bg-9-271-2012, 2012.

617 [Honrath, R.E., Owen, R.C., Val Martin, M., et al. 2004. Regional and hemispheric impacts of](#)
618 [anthropogenic and biomass burning emissions on summertime CO and O₃ in the North Atlantic](#)
619 [lower free troposphere. *Journal of Geophysical Research: Atmospheres*, 109\(D24\), doi:](#)
620 [10.1029/2004JD005147.](#)

621 Jacob, D.J., and Winner, D.A.: Effect of climate change on air quality, *Atmospheric Environment*, 43
622 (1), 51-63, doi:10.1016/j.atmosenv.2008.09.051, 2009.

623 Jerrett, M., Burnett, R.T., Pope, C.A., et al.: Long-term ozone exposure and mortality, *The New*
624 *England Journal of Medicine*, 360 (11), 1085–1095, doi: 10.1056/NEJMoa0803894, 2009.

625 Kaiser, J.W., Hell, A., Andreae, M.O., et al.: Biomass burning emissions estimated with a global fire
626 assimilation system based on observed fire radiative power, *Biogeosciences*, 9(1), 527–554, doi:
627 10.5194/bg-9-527-2012, 2012.

628 Lhotka, O., Kysely, J. and Farda, A.: Climate change scenarios of heat waves in Central Europe and
629 their uncertainties, *Theoretical and Applied Climatology*, 131, 1043-1054, doi: 10.1007/s00704-016-
630 2031-3, 2017.

631 Li, M., Yao, Y., Simmonds, I., et al.: Collaborative impact of the NAO and atmospheric blocking on
632 European heat waves, with a focus on the hot summer of 2018, *Environmental Research Letters*, 15,
633 114003, doi:10.1088/1748-9326/aba6ad, 2020.

634 Liu, X., He, B., Guo, L., et al.: Similarities and differences in the mechanisms causing the European
635 summer heat waves in 2003, 2010 and 2018, *Earth's Future*, e2019EF001386, doi:
636 10.1029/2019EF001386, 2020.

637 Mann, G.W., Carslaw, K.S., Spracklen, D.V., et al.: Description and evaluation of GLOMAP-mode: A
638 modal global aerosol microphysics model for the UKCA composition-climate model. *Geoscientific*
639 *Model Development*, 3(2), 519–551, doi:10.5194/gmd-3-519-2010, 2010.

640 Matsueda, M.: Predictability of Euro-Russian blocking in summer of 2010, *Geophysical Research*
641 *Letters*, 38, L06801, doi:10.1029/2010GL046557, 2011.

642 Methven, J., Arnold, S.R., O'Connor, F.M., et al.: Estimating photochemically produced ozone
643 throughout a domain using flight data and a Lagrangian model, *Journal of Geophysical Research:*
644 *Atmospheres*, 10 (D9), doi:10.1029/2002JD002955, 2003.

645 Miles, G.M., Siddans, R., Kerridge, B. J., Latter, B. G., and Richards, N. A. D.: Tropospheric ozone and
646 ozone profiles retrieved from GOME-2 and their validation, *Atmospheric Measurement Techniques*,
647 8, 385–398, doi:10.5194/amt-8-385-2015, 2015.

648 Monks, S.A., Arnold, S.R., Hollaway, M. J., et al.: The TOMCAT global chemistry transport model v1.6:
649 Description of chemical mechanism and model evaluation, *Geoscientific Model Development*, 10 (8),
650 3025–3057, doi:10.5194/gmd-10-3025-2017, 2017.

651 Morgenstern, O., Hegglin, M.I., Rozanov, E., et al.: Review of the global models used with phase 1 of
652 the Chemistry-Climate Model Initiative (CCMI), *Geoscientific Model Development*, 10 (2), 639–671,
653 doi:10.5194/gmd-10-639-2017, 2017.

654 Munro, R., Siddans, R., Reburn, W. J., and Kerridge, B. J.: Direct measurement of tropospheric ozone
655 distributions from space, *Nature*, 392, 168–171, doi:10.1038/32392, 1998.

656 Pacifico, F., Harrison, S.P., Jones, C.D., et al.: Evaluation of a photosynthesis-based biogenic isoprene
657 emission scheme in JULES and simulation of isoprene emissions under present-day climate
658 conditions, *Atmospheric Chemistry and Physics*, 11, 4371–4389, doi:10.5194/acp-11-4371-2011,
659 2011.

660 Palmer, P., I., Marvin, M., R., Siddans, R., et al.: Nocturnal survival of isoprene linked to formation
661 of upper tropospheric organic aerosol, *Science*, 375 (6580), 562-566,
662 doi:10.1126/science.abg4506.

663 [Papanastasiou, D.K., Melas, D. and Kambezidis, H.D., 2015. Air quality and thermal comfort levels](#)
664 [under extreme hot weather. *Atmospheric Research*, 152, 4-13, doi:](#)
665 [10.1016/j.atmosres.2014.06.002.](#)

666 PHE (Public Health England), PHE heatwave mortality monitoring, available at:
667 [https://assets.publishing.service.gov.uk/government/uploads/system/uploads/attachment_data/file](https://assets.publishing.service.gov.uk/government/uploads/system/uploads/attachment_data/file/942648/PHE_heatwave_report_2018.pdf)
668 [/942648/PHE_heatwave_report_2018.pdf](https://assets.publishing.service.gov.uk/government/uploads/system/uploads/attachment_data/file/942648/PHE_heatwave_report_2018.pdf) (last accessed 3rd February 2022), 2019.

669 [Pimlott, M.A., Pope, R.P., Kerridge, B.J., et al.: Investigating the global OH radical distribution using](#)
670 [steady-state approximations and satellite data. *Atmospheric Chemistry and Physics*, 22, 10467-](#)
671 [10488, doi: 10.5194/acp-22-10467-2022, 2022.](#)

672 Pirovano, G., Balzarini, A., Bessagnet, B., et al.: Investigating impacts of chemistry and transport
673 model formulation on model performance at European scale, *Atmospheric Environment*, 53, 93–109,
674 doi:10.1016/j.atmosenv.2011.12.052, 2012.

675 Pope, R.J., Savage, N.H., Chipperfield, M.P., et al.: The influence of synoptic weather regimes on UK
676 air quality: analysis of satellite column NO₂, *Atmospheric Science Letters*, 15, 211– 217,
677 doi:10.1002/asl22.492, 2014.

678 Pope, R.J., Butt, E.W., Chipperfield, M.P., et al.: The impact of synoptic weather on UK surface ozone
679 and implications for premature mortality. *Environmental Research Letters*, 11, 124004,
680 doi:10.1088/1748-9326/11/12/124004, 2016.

681 [Pope, R.J., Chipperfield, M.P., Arnold, S.R., et al. 2018. Influence of the wintertime North Atlantic](#)
682 [Oscillation on European tropospheric composition: an observational and modelling study.](#)
683 [Atmospheric Chemistry and Physics, 18, 8389–8408, doi: 10.5194/acp-18-8389-2018.](#)

684 Pope, R.J., Arnold, S.R., Chipperfield, M.P., et al.: Substantial Increases in Eastern Amazon and
685 Cerrado Biomass Burning-Sourced Tropospheric Ozone. *Geophysical Research Letters*, 47 (3),
686 e2019GL084143, doi:10.1029/2019GL084143, 2020.

687 Pope, R. J., Kerridge, B. J., Siddans, R., et al.: Large enhancements in southern hemisphere satellite-
688 observed trace gases due to the 2019/2020 Australian wildfires, *Journal of Geophysical Research:*
689 *Atmospheres*, 1–13, doi:10.1029/2021jd034892, 2021.

690 Pyrgou, A., Hadjinicolaou, P and Santamouris, M: Enhanced near-surface ozone under heatwave
691 conditions in a Mediterranean island, *Scientific Reports*, 8, 9191, doi:10.1038/s41598-018-27590-z,
692 2018.

693 RAL Space, Optimal Estimation Method retrievals with IASI, AMSU and MHS – Final Report Version
694 5.2, available at: http://cedadocs.ceda.ac.uk/1377/1/iasi_mhs_final_report_v5p2.pdf (last accessed
695 17/08/2020), 2015.

696 [Rasilla, D., Allende, F., Martilli, A., et al. 2019. Heat Waves and Human Well-Being in Madrid](#)
697 [\(Spain\). *Atmosphere*, 10\(5\), 288-309, doi: 10.3390/atmos10050288.](#)

698 Rebetez, M., Dupont, O. and Giroud, M.: An analysis of July 2006 heatwave extent in Europe
699 compared to the record year of 2003, *Theoretical and Applied Climatology*, 95, 1-7,
700 doi:10.1007/s00704-007-0370-9, 2008.

701 [Rennenberg, H., Loreto, F., Polle, A., et al. 2006. Physiological Responses of Forest Trees to Heat and](#)
702 [Drought. *Plant Biology*, 8\(5\), 556-571, doi: 10.1055/s-2006-924084.](#)

703 Richards, N.A.D, Arnold, S.R., Chipperfield, M.P., et al.: The Mediterranean summertime ozone
704 maximum: global emission sensitivities and radiative impacts, *Atmospheric Chemistry and Physics*,
705 13, 2231-2345, doi:10.5194/acp-13-2331-2013, 2013.

706 Riese, M., Ploeger, F., Rap, A., et al.: Impacts of uncertainties in atmospheric mixing on simulated
707 UTLS composition and related radiative effects, *Journal of Geophysical Research: Atmospheres*, 117,
708 D16305, doi:10.1029/2012jd017751, 2012.

709 Rodgers, C.D.: Inverse methods for atmospheric sounding: Theory and practice. New Jersey, USA:
710 World Science. 2000.

711 [Roelofs, G.L., Kentarchos, A.S., Trickl, T., et al. 2003. Intercomparison of tropospheric ozone models:](#)
712 [Ozone transport in a complex tropopause folding event. *Journal of Geophysical Research*, 108 \(D12\),](#)
713 [8529, doi: 10.5194/acp-19-14387-2019.](#)

714 [Schultz, M.G., Schroder, S., Lyapina, O., et al. 2017. Tropospheric Ozone Assessment Report:](#)
715 [Database and metrics data of global surface ozone observations. *Elementa – Science of the*](#)
716 [Anthropocene, 5\(58\), doi: 10.1525/elementa.244.](#)

717 Scott, P.A., Stone, D.A. and Allen, M.R.: Human contributions to the European heatwave of 2003,
718 *Nature*, 432, 610-614, doi:10.1038/nature03089, 2004.

719 Sitch, S., Cox, P.M., Collins, W.J., & Huntingford, C.: Indirect radiative forcing of climate change
720 through ozone effects on the land carbon sink, *Nature*, 448, 791–795, doi:10.1038/nature06059,
721 2007.

722 Smith, N.E., Kooijmans, L.M.J., Koren, G., et al.: Spring enhancements and summer reduction in
723 carbon uptake during the 2018 drought in Northwestern Europe, *Philosophical Transactions B*, 375,
724 20190509, doi:10.1098/rstb.2019.0509, 2020.

725 [Stockwell, D., Giannakopoulos, C., Plantevin, P.-H., et al. 1999. Modelling NO_x from lightning and its
726 impact on global chemical fields. *Atmospheric Environment*, **33**, 4477–4493, doi: 10.1016/S1352-
727 2310\(99\)00190-9.](#)

728 Thomas, M.A. and Devasthale, A.: Sensitivity of free tropospheric carbon monoxide to atmospheric
729 weather states and their persistency: an observational assessment over the Nordic countries,
730 *Atmospheric Chemistry and Physics*, 14, 11545–11555, doi:10.5194/acp14-11545-2014, 2014.

731 Van Dingenen, R., Dentener, F.J., Raes, F., et al.: The global impact of ozone on agriculture crop
732 yields under current and future air quality legislation. *Atmospheric Environment*, 43(3), 604–618,
733 doi:10.1016/j.atmosenv.2008.10.033, 2009.

734 Vieno, M., Dore, A.J., Stevenson, D.S., et al.: Modelling surface ozone during the 2003 heat-wave in
735 the UK, *Atmospheric Chemistry and Physics*, 10, 7963–7978, doi:10.5194/acp-10-7963-2010, 2010.

736 WHO (World Health Organisation), Ambient (outdoor) air pollution, available at:
737 [https://www.who.int/news-room/fact-sheets/detail/ambient-\(outdoor\)-air-quality-and-health](https://www.who.int/news-room/fact-sheets/detail/ambient-(outdoor)-air-quality-and-health) (last
738 accessed 3rd February 2022), 2021.

739

740

741

742

743

744

745

746

747

748

749

750

751

752

753

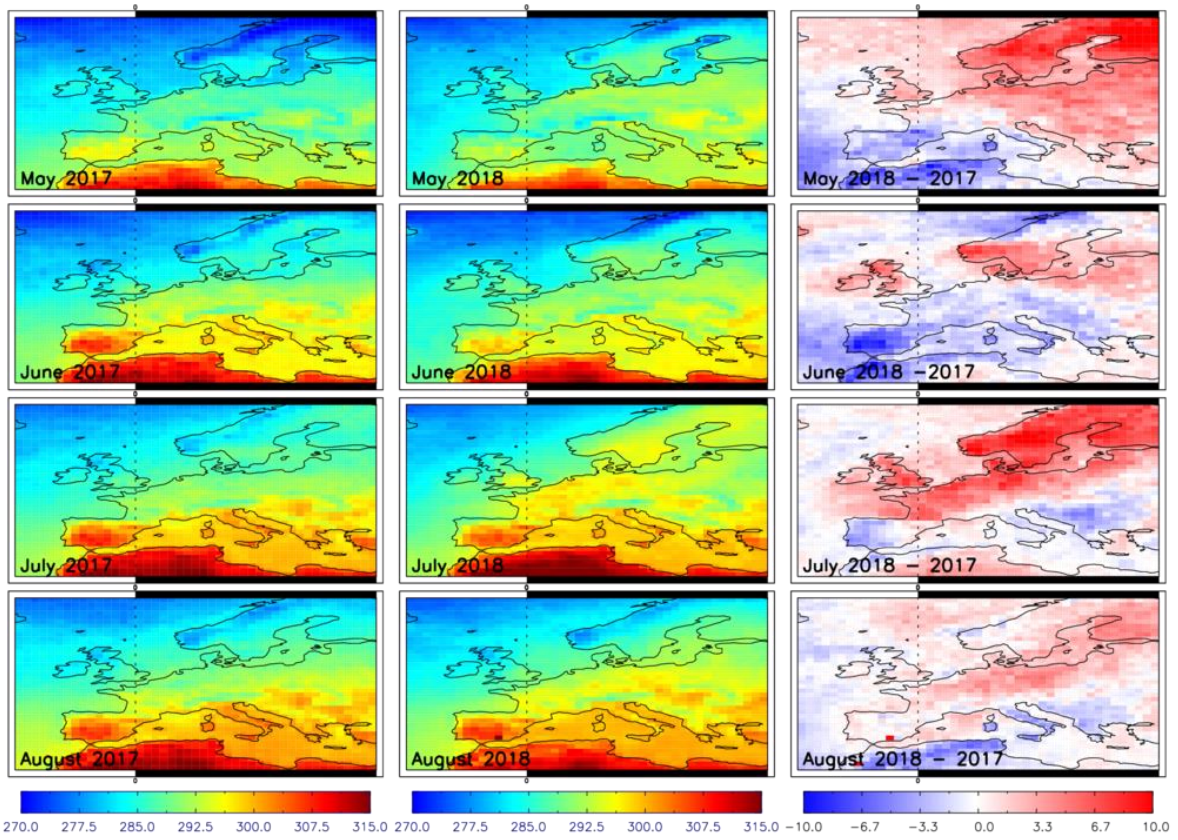
754

755

756

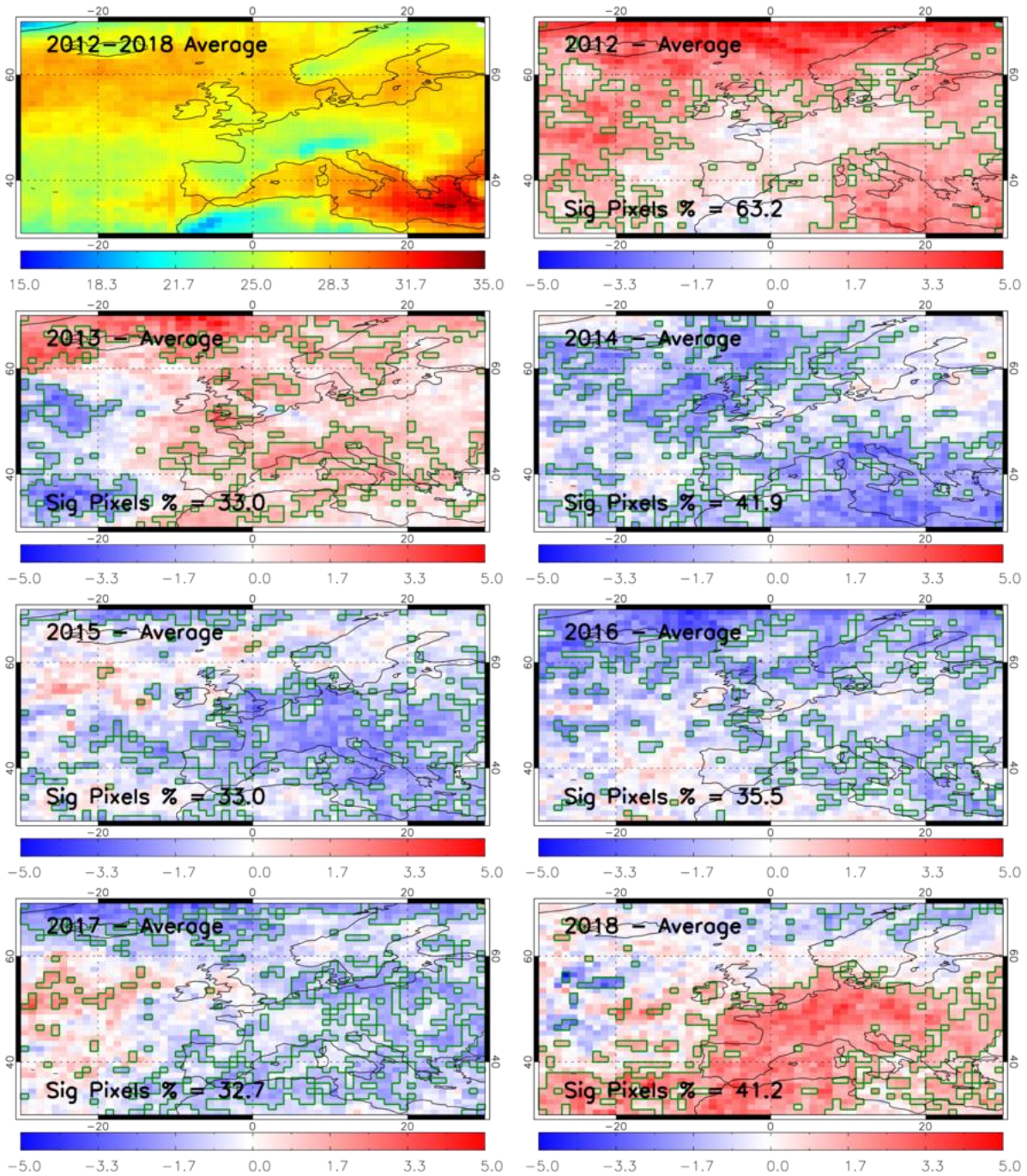
757

758 Figures:



759
760
761
762
763

Figure 1: Surface temperature (K) over Europe for May to August in 2017 (LHS left column), 2018 (middle centre column) and 2018-2017 difference (RHS right column) retrieved from MetOp-A IASI, MHS and AMSU by the IMS scheme.



764

765

766

767

768

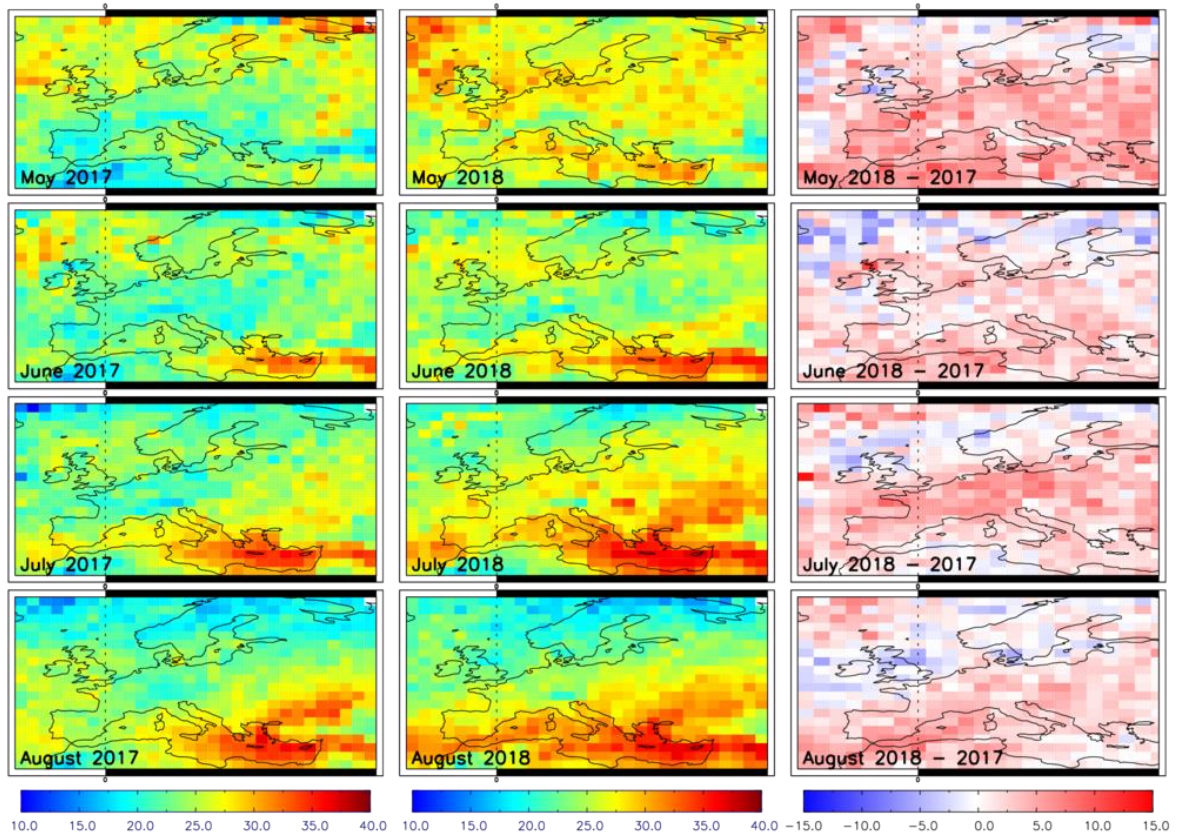
769

770

771

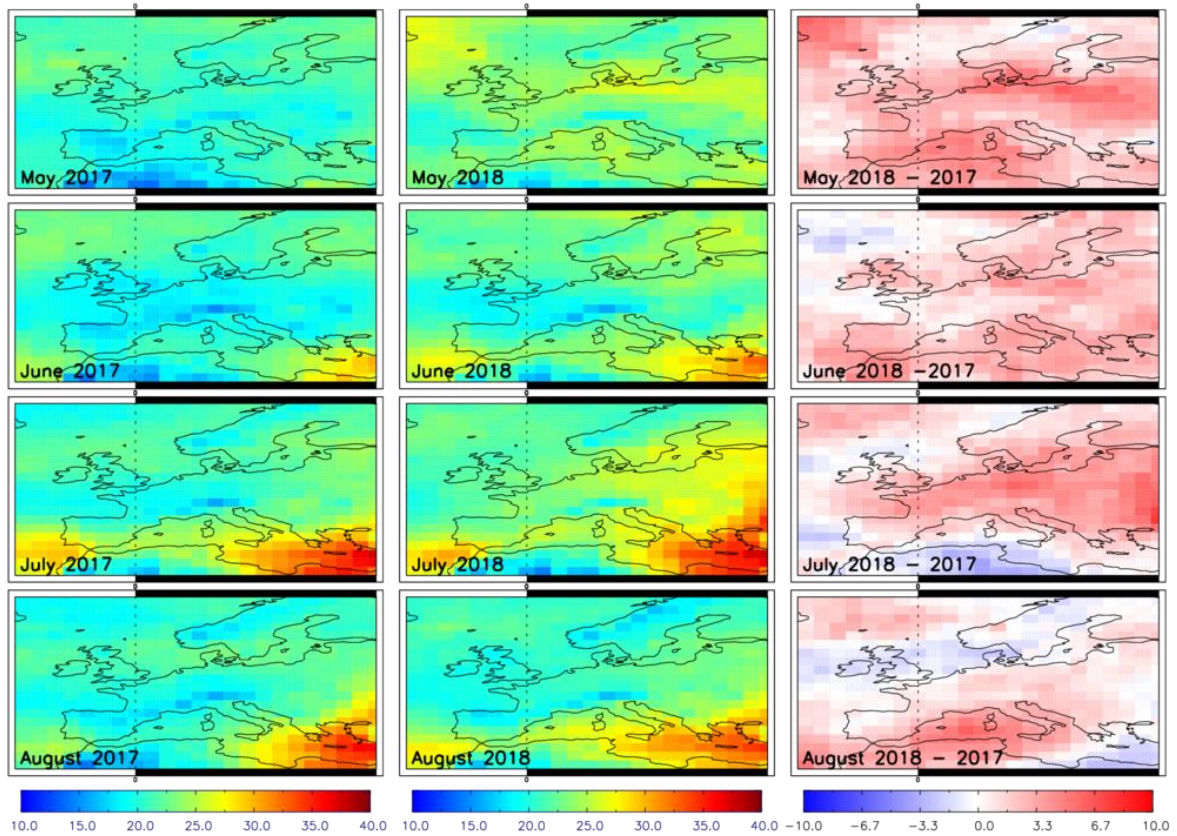
772

Figure 2: Sub-column ozone (SCO_3 , surface-450 hPa), in Dobson units (DU), retrieved from GOME-2 on Metop-A averaged across May to August between 2012 and 2018 (top left panel) and the corresponding difference from the 2012-18 mean for each year, respectively. The green-polygon-outlined regions show where the year-specific seasonal average is significantly different (95% confidence level based on the Wilcoxon Rank Test (WRT)) from the long-term (2012-2018) seasonal average. The "Sig Pixel %" label indicates the number of pixels in the domain with significant differences.



773
 774
 775
 776

Figure 3: SCO_3 (DU) from GOME-2 over Europe for May to August in (left column) 2017, (*middle* *centre* column) 2018 and (right column) 2018-2017 difference.



777

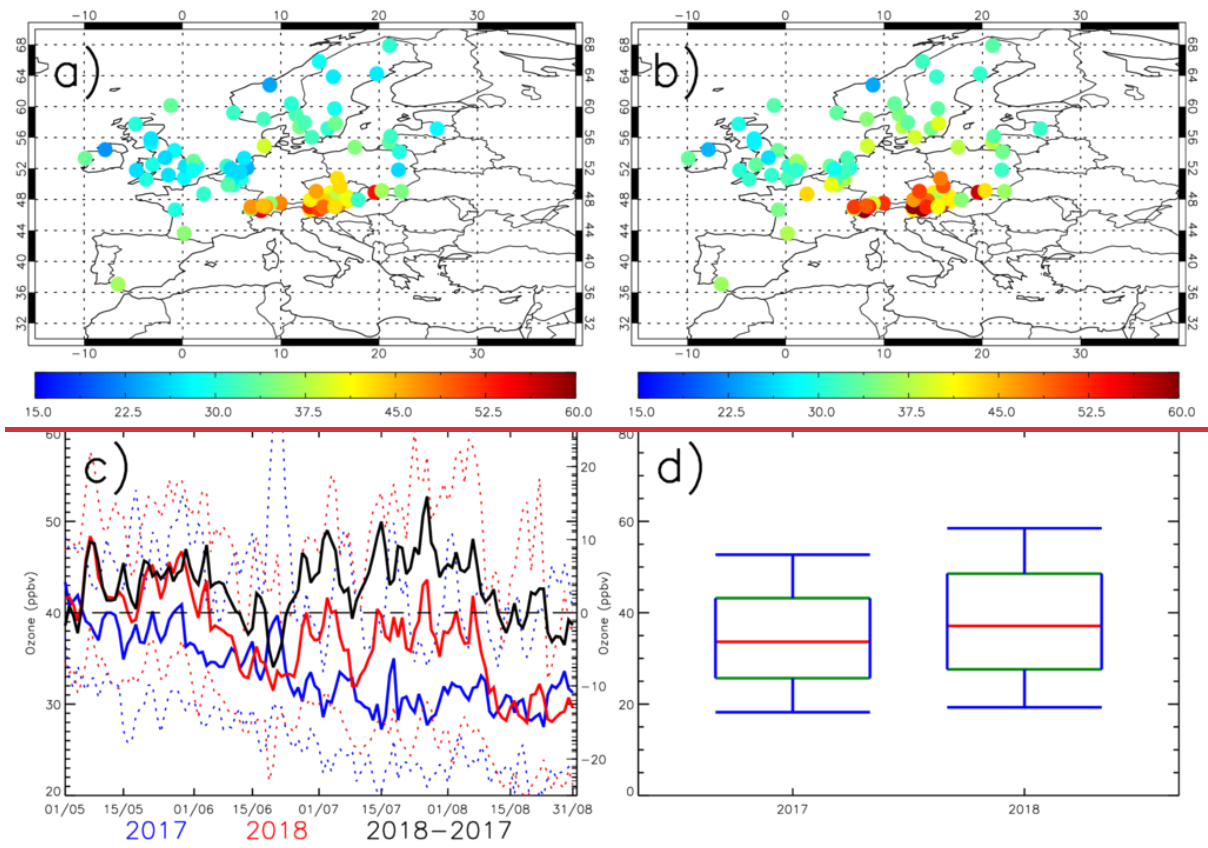
778

779

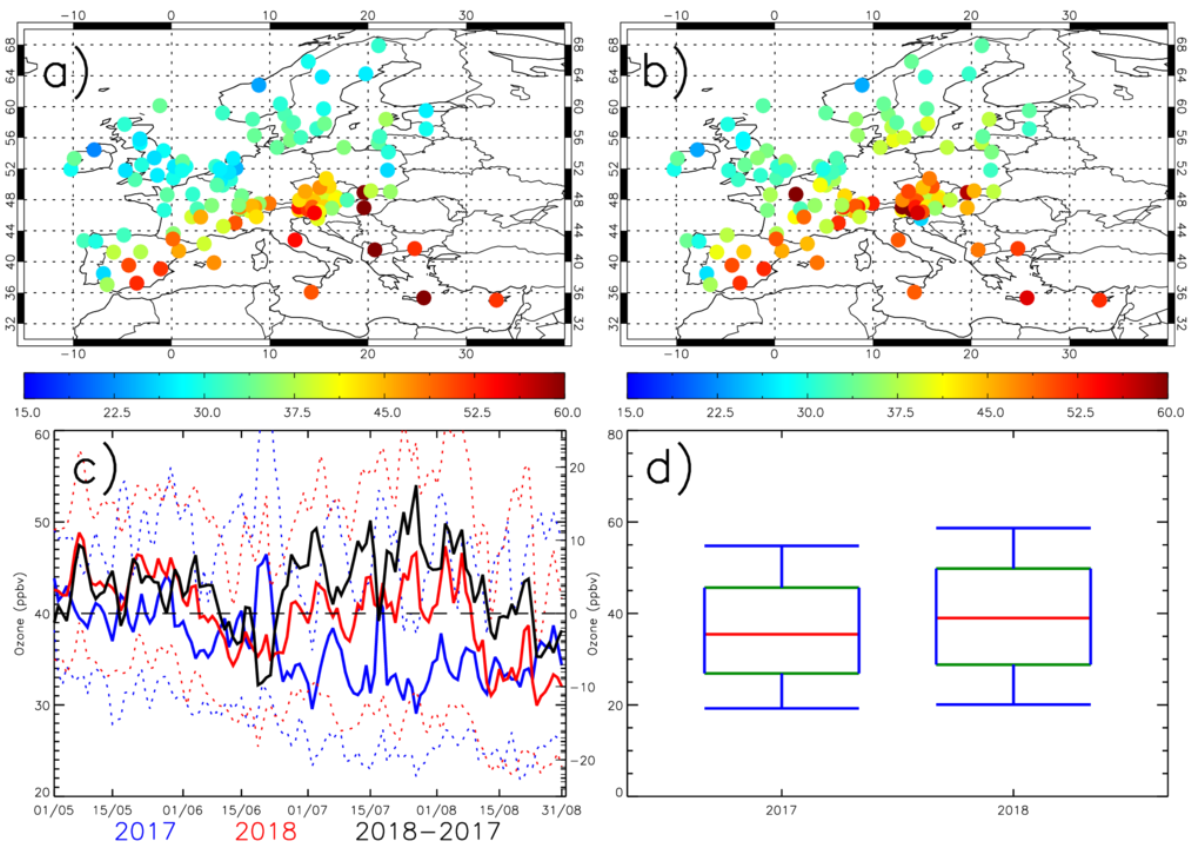
780

781

Figure 4: SCO_3 (DU) for May to August in 2017 (LHSleft column), 2018 (middlecentre column) and 2018-2017 difference (RHSright column) over Europe retrieved from MetOp-A IASI, MHS and AMSU by the IMS scheme.



782



783

784

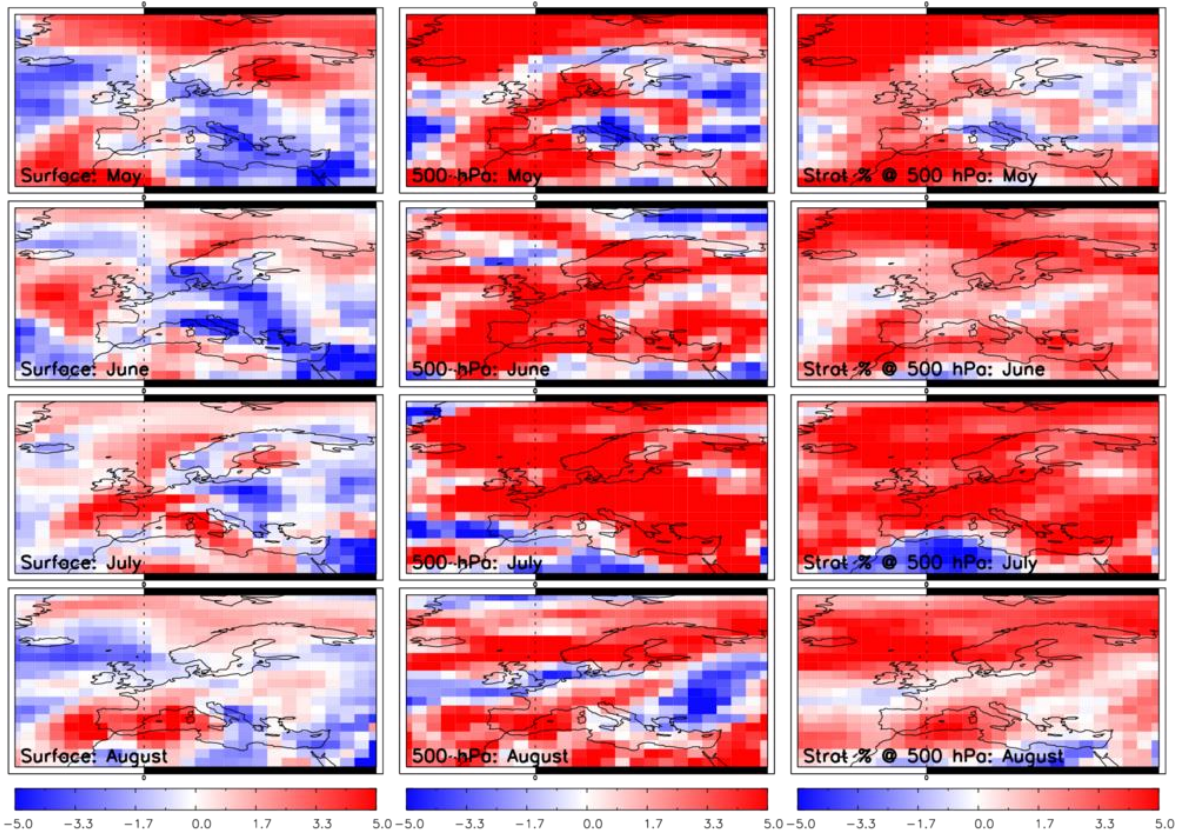
785

Figure 5: European surface ozone (ppbv) for a) May-June-July-August (MJJA) 2017, b) MJJA 2018), c) regional mean time series (dotted lines show mean \pm standard deviation) for MJJA 2017 (blue), MJJA

786 2018 (red) and the 2018-2017 difference (black) and d) box-whisker plots for MJA 2017 and 2018. In
 787 panel d) the median, 25th & 75th percentiles and 10th & 90th percentiles are shown by the red, green
 788 and blue lines, respectively.

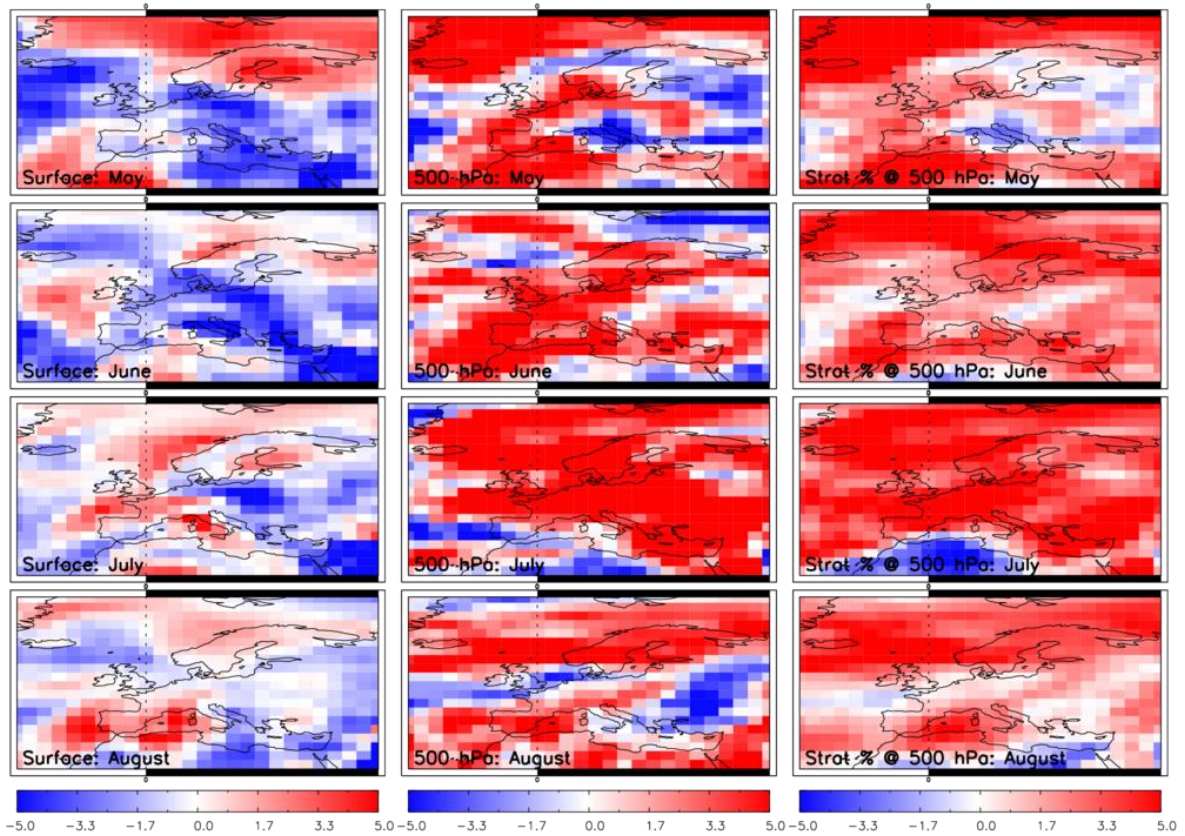
789 **Figure 5:** European surface ozone (ppbv) for a) May June July August (MJA) 2017, b) MJA 2018), c)
 790 regional time-series for MJA 2017 (blue), MJA 2018 (red) and the 2018-2017 difference (black) and
 791 d) box-whisker plots for MJA 2017 and 2018. In panel d) the median, 25th & 75th percentiles and
 792 10th & 90th percentiles are shown by the red, green and blue lines, respectively.

793



794 **Figure 6:** TOMCAT ozone (ppbv) 2018-2017 differences for May to August for the surface (LHSleft
 795 column), 500 hPa (middlecentre column) and the stratospheric contribution (%) to the 500 hPa layer
 796 (RHSright column).

798



799

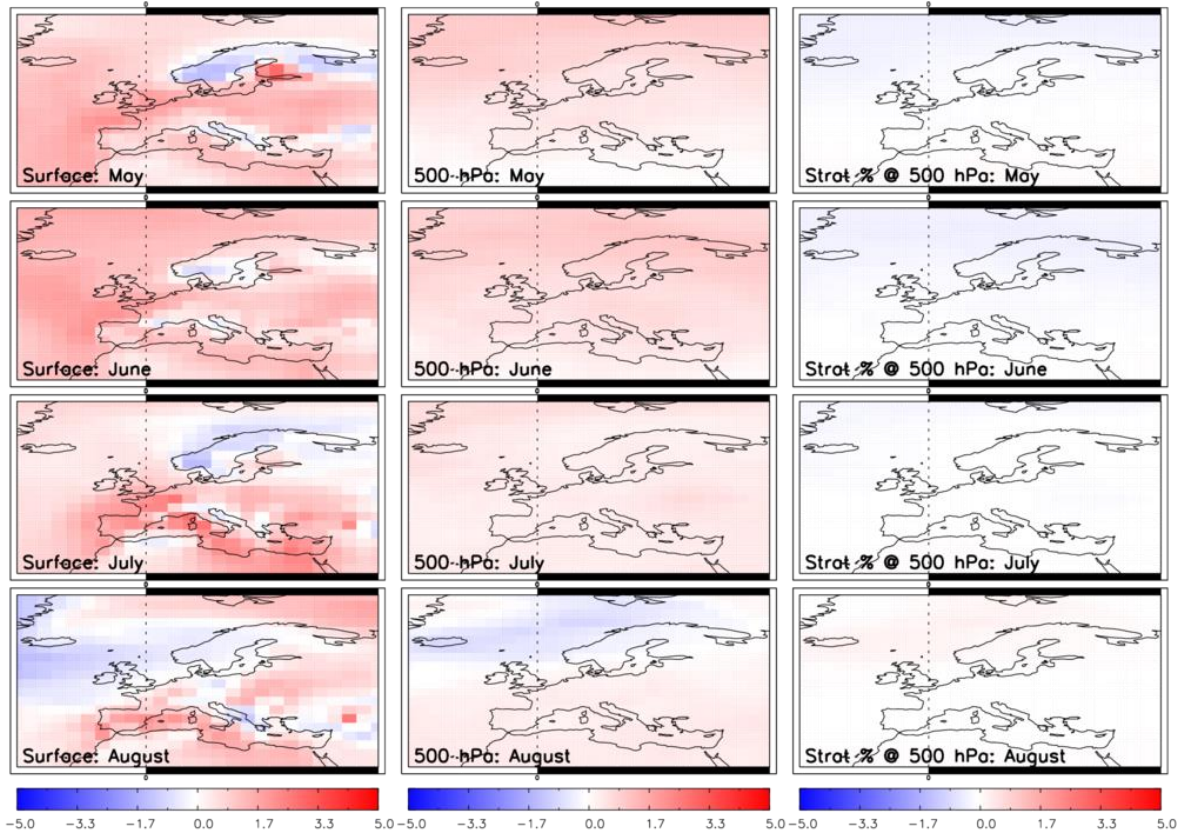
800

801

802

803

Figure 7: TOMCAT ozone (ppbv) 2018-2017 differences for May to August for the fixed emissions simulation (Fixed_EMIS) for the surface (LHSleft column), 500 hPa (middlecentre column) and the stratospheric contribution (%) to the 500 hPa layer (RHSright column).



804

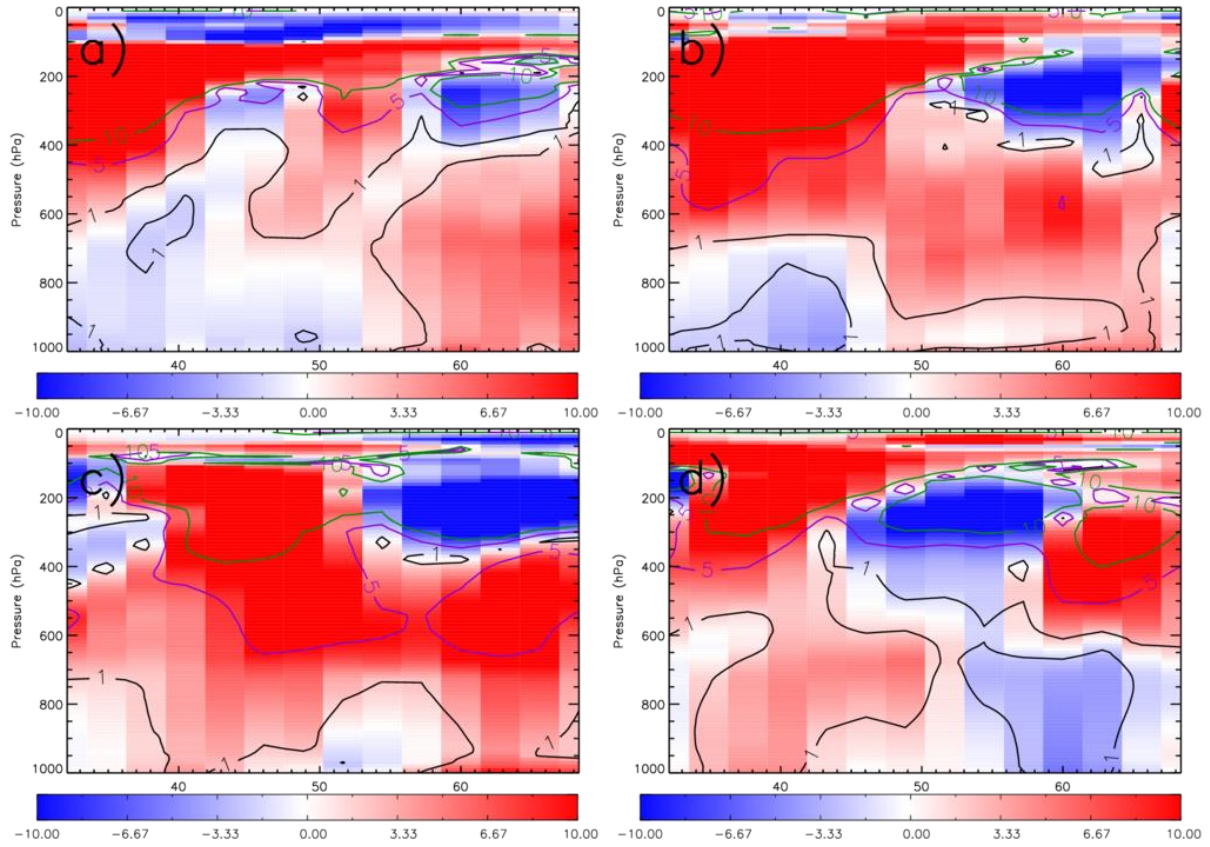
805 **Figure 8:** TOMCAT ozone (ppbv) 2018-2017 differences for May to August for the fixed meteorology
 806 simulation (Fixed_MET) for the surface (LHSleft column), 500 hPa (middlecentre column) and the
 807 stratospheric contribution (%) to the 500 hPa layer (RHSright column).

808

809

810

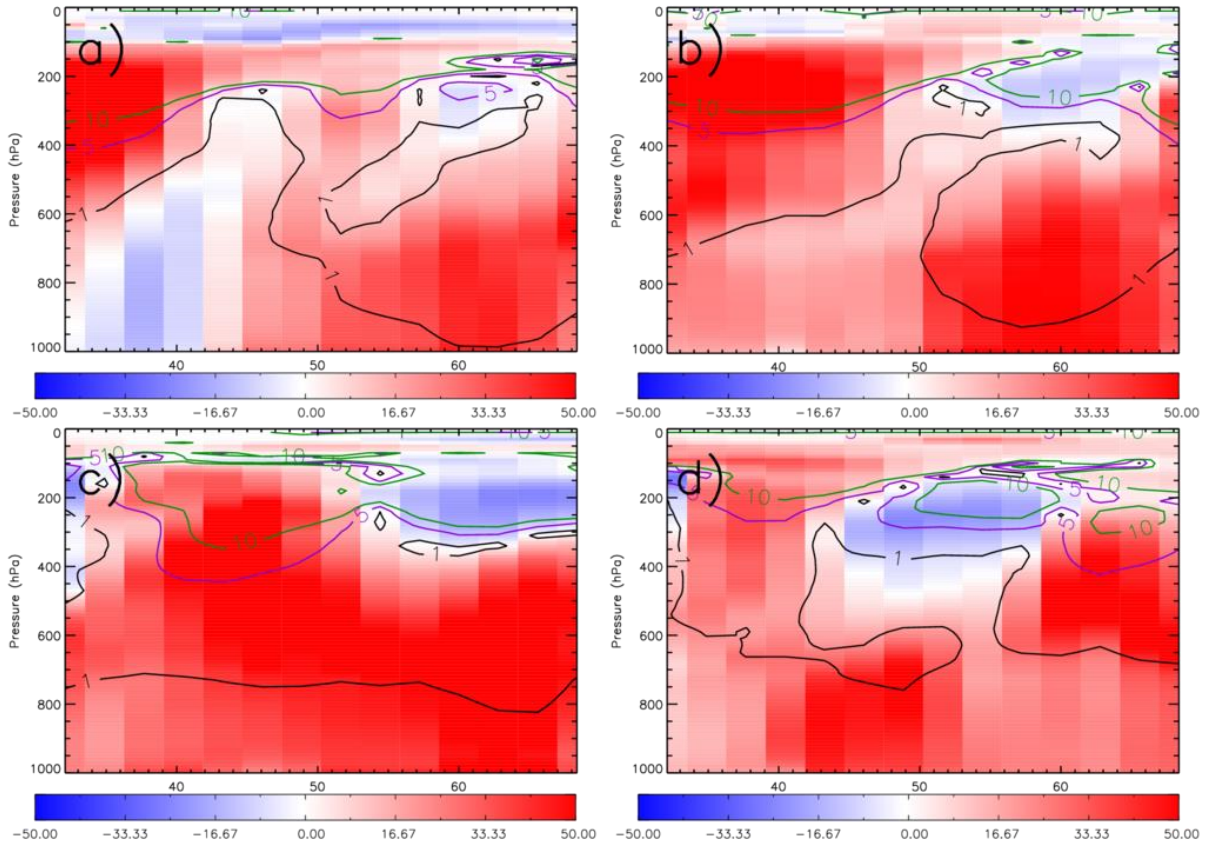
811



812

813 **Figure 9:** TOMCAT ozone, zonally averaged between 20°W and 40°E, 2018-2017 percentage
 814 differences (absolute difference (ppbv) shown as solid lines) from the control simulation. Panels a)-d)
 815 represent the monthly averages for May, June, July and August.

816



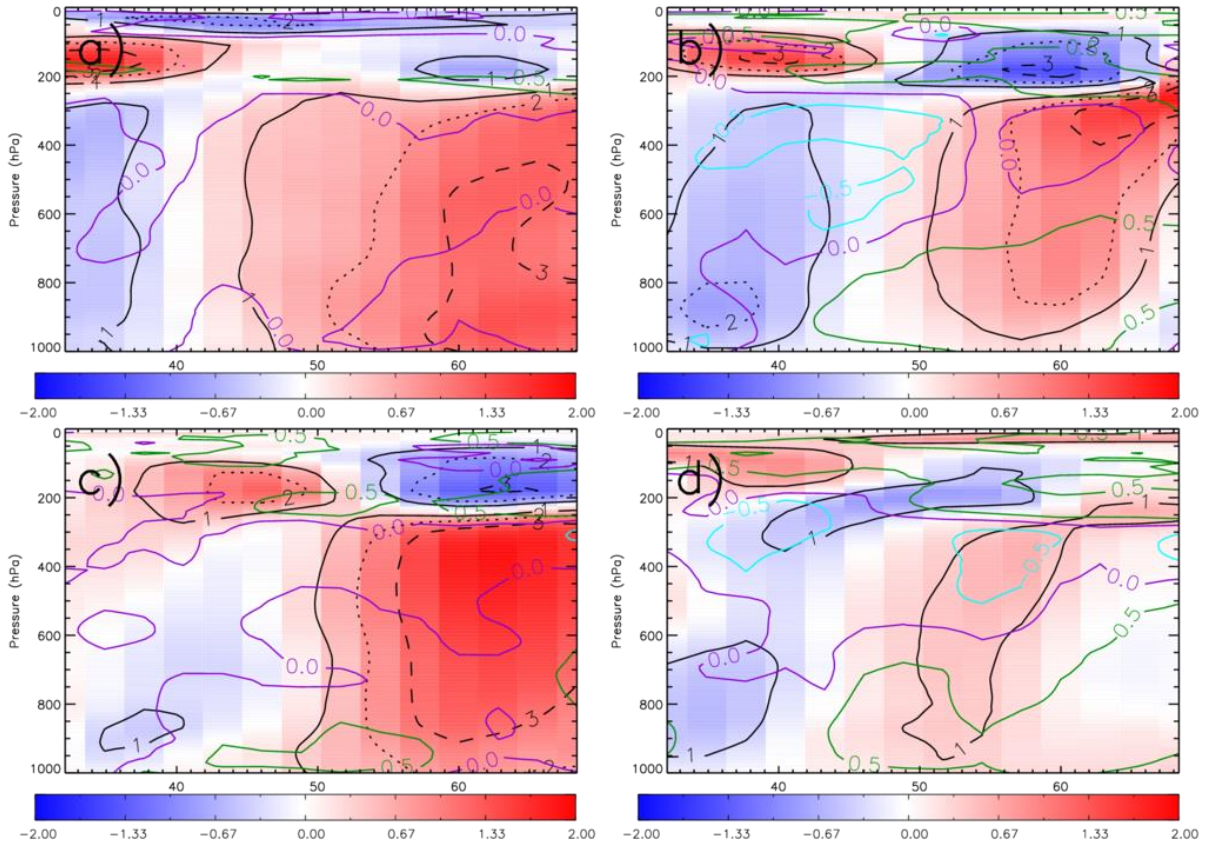
817

818 **Figure 10:** TOMCAT stratospheric ozone tracer, zonally averaged between 20°W and 40°E, 2018-2017
 819 percentage differences (absolute difference (ppbv) shown as solid lines) from the control simulation.
 820 Panels a)-d) represent the monthly averages for May, June, July and August.

821

822

823



824

825 **Figure 11:** TOMCAT temperature, zonally averaged between 20°W and 40°E, 2018-2017 percentage
 826 differences (absolute difference (K) shown by black solid, dotted and dashed lines) from the control
 827 simulation. Overplotted are contours of the temporal correlation (i.e. within each grid box) between
 828 the temperature and ozone 2018-2017 differences. Panels a)-d) represent the monthly averages for
 829 May, June, July and August.

830

831

832

833

834

835

836

837

838

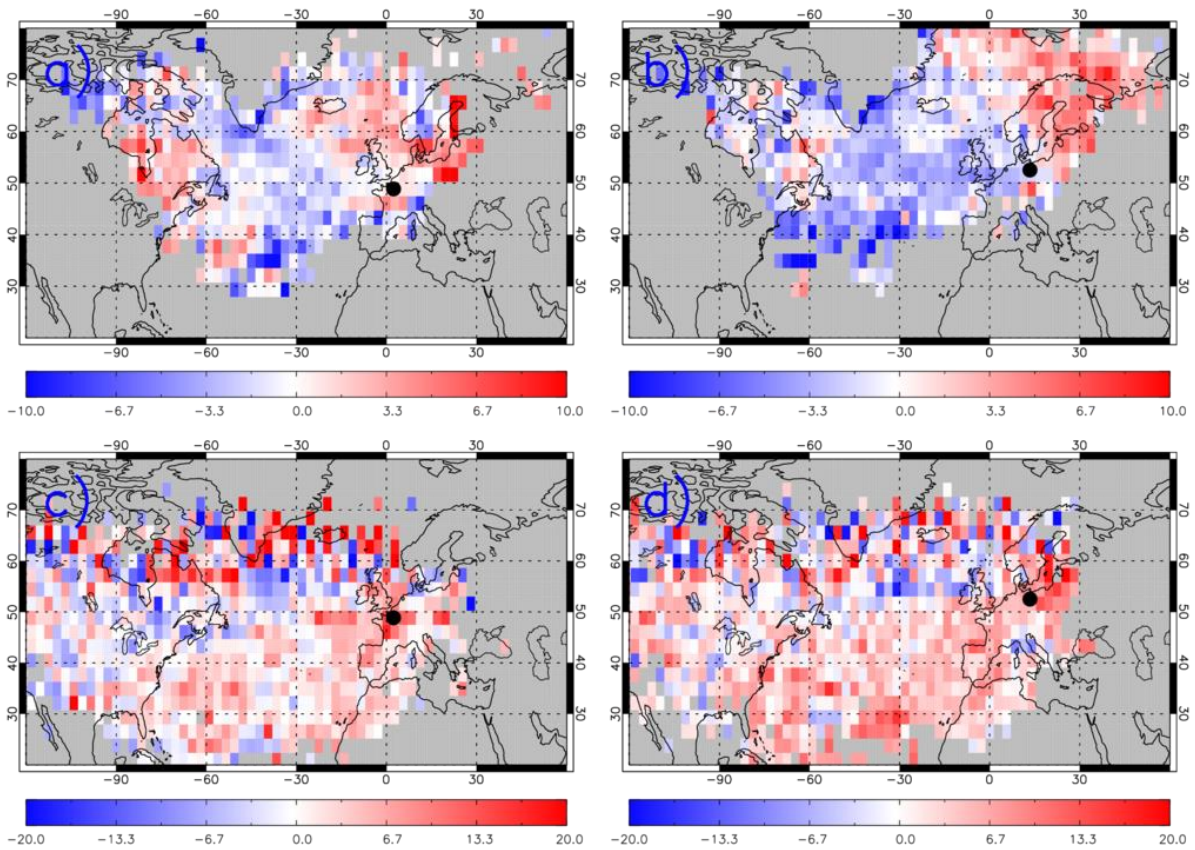
839

840

841

842

843



844

845 **Figure 12:** The difference between May-August 2018 and May-August 2017 (i.e. 2018-2017) ROTRAJ
846 back-trajectories (10 days), weighted by the average TOMCAT O₃ (ppbv) concentration along each
847 trajectory path, gridded onto the TOMCAT horizontal resolution for a) Paris at the surface, b) Berlin
848 at the surface, c) Paris at approximately 500 hPa and d) Berlin at approximately 500 hPa. The black
849 circles represent the location of Paris or Berlin, where the trajectories were released from.

850